Title: Synergic activity of FGFR2 and MEK inhibitors in the treatment of FGFR2-amplified cancers of unknown primary

Authors: *Andrea Cavazzoni[1†], Irene Salamon[2†], Claudia Fumarola[1†], Giulia Gallerani[2], Noemi Laprovitera[3], Francesco Gelsomino[3], Mattia Riefolo[2,3], Karim Rihawi[3], Elisa Porcellini[2], Tania Rossi[4], Martina Mazzeschi[2], Maria Naddeo[2,3], Salvatore Serravalle[3], Elisabetta Broseghini[2], Federico Agostinis[5‡], Olivier Deas[6], Roberta Roncarati[1,7], Giorgio Durante[2], Mattia Lauriola[2], Ingrid Garajova[8], George A. Calin[9], Massimiliano Bonafè[2,3], Antonia D'Errico[2,3], Pier Giorgio Petronini[1], Stefano Cairo[6§], Andrea Ardizzoni[2,3], Gabriele Sales[5$] and Manuela Ferracin[2,3$]**

Affiliations:

[1] Department of Medicine and Surgery, University of Parma; Parma, Italy.

[2] Department of Medical and Surgical Sciences (DIMEC), University of Bologna; Bologna, Italy.

[3] IRCCS, Azienda Ospedaliero-Universitaria di Bologna; Bologna, Italy.

[4] Istituto Scientifico Romagnolo per lo Studio e la Cura dei Tumori (IRST) IRCCS; Meldola (FC), Italy.

[5] Department of Biology, University of Padova; Padua, Italy.

[6] XenTech; Evry, France.

[7] Istituto di Genetica Molecolare "Luigi Luca Cavalli-Sforza" - Consiglio Nazionale delle Ricerche (CNR), Bologna, Italy.

[8] Medical Oncology Unit, University Hospital of Parma; Parma, Italy.

[9] Department of Experimental Therapeutics, The University of Texas MD Anderson Cancer Center; Houston, TX 77030, USA.

† These authors contributed equally

$ Equal co-last authorship

‡ FA is currently an Associate Data Analyst & Data Scientist at Evotec SE (Hamburg, Germany)

§ SC is currently senior global scientific director at Champions Oncology (USA)

* Correspondence should be addressed to: Manuela Ferracin

Via S. Giacomo, 14 40126 Bologna

+39 051 2094714 manuela.ferracin@unibo.it

Short title: Synergic activity of FGFR2 and MEK inhibitors in CUP models (59)

Abstract

Patients with cancer of unknown primary (CUP) carry the burden of an aggressive disease and reduced access to therapies. Experimental models are pivotal for CUP biology investigation and drug testing. We derived two CUP cell lines (CUP#55 and #96), and corresponding patient-derived xenografts (PDXs), from ascites tumor cells. CUP cell lines and PDXs underwent histological, immune-phenotypical, molecular, and genomic characterization confirming the features of the original tumor. The tissue-of-origin prediction was obtained from the tumor microRNA expression profile and confirmed by single-cell transcriptomics. Genomic testing and FISH analysis identified FGFR2 gene amplification in both models, in the form of homogenously staining region (HSR) in CUP#55 and double minutes in CUP#96. FGFR2 was recognized as the main oncogenic driver and therapeutic target. FGFR2-targeting drug BGJ-398 (infigratinib) in combination with the MEK inhibitor trametinib proved to be synergic and exceptionally active, both *in vitro* and *in vivo*. The effects of the combined treatment by single-cell gene expression analysis revealed a remarkable plasticity of tumor cells and the greater sensitivity of cells with epithelial phenotype. This study brings personalized therapy closer to CUP patients and provides the rationale for FGFR2 and MEK targeting in metastatic tumors with FGFR2 pathway activation.

INTRODUCTION

Metastases develop when tumor cells spread from the primary site to surrounding or distant tissues and are responsible for 90% of cancer-related deaths (1). Among metastatic patients, 3-5% show no clinical evidence of a primary site at diagnosis. These cases are classified as cancers of uncertain origin or cancers of unknown primary site (CUPs) or occult primary tumors (2) (3). They are usually diagnosed at a late stage, with patients presenting one or more metastases already at first diagnosis. The identification of tumor primary site is usually obtained by a combination of diagnostic

investigations including physical examinations, blood analyses, imaging and immunohistochemical (IHC) testing of the tumor tissue. In CUP patients, these investigations are inconclusive.

International guidelines for tumor treatment are based on primary site indication. Therefore, CUP treatment requires a blind approach, which is very challenging for oncologists. Consequently, CUPs are typically treated with empiric platinum-based chemotherapy regimens, which are usually poorly effective. Indeed, CUP patients have a short life-expectancy (average overall survival 4-9 months, with only 20% surviving more than 1 year) which, unfortunately, did not improve over the last decades. However, these regimens remain empirical since they are mostly based on results of single-arm phase II clinical trials (4) (5) (6) or small phase III trials (7) (8) (9).

The use of molecular tests based on gene/miRNA expression signatures or methylation profiles to identify the most probable site-of-origin could assist the oncologists in the selection of the best treatment options and potentially improve CUPs outcome (10) (11). NCCN guidelines for occult primary tumors recently introduced the recommendation to use NGS genetic testing to guide therapeutic decision (v.2/2023) and suggest 11 different chemotherapy regimens for adenocarcinoma and 9 for squamous histology.

With the advent of personalized medicine, patient management is more and more frequently associated with the identification of specific molecular or genetic features of the tumor upon which therapies could be based to avoid suboptimal treatments. The identification of druggable alterations in CUP tumors could increase the otherwise limited treatment options, as recently demonstrated by Hayashi et al. (12). Next generation sequencing technologies were applied to the analysis of CUP mutational profile (13) (14) (15) (16) (17). Overall, CUPs seem to harbor recognized actionable genetic alterations in nearly 30% of cases (3) (18). Immunotherapy has been scarcely tested on CUP patients: in a study by Gatalica et al. only a fraction of patients presented favorable biomarkers for the use of immune checkpoint inhibitors (19). Varghese et al. identified the actionable mutations in a dataset of 150 CUPs analyzed with the MSK-IMPACT panel and patients who were treated with targeted therapies, showed clinical benefit and longer survival (15). A meta-analysis conducted by

86 Ding et al. confirmed a benefit for site-specific therapies only for CUP patients with a stronger
87 primary site prediction (20).
88 However, the knowledge that molecular and genetic testing could provide novel personalized
89 treatments for CUP patients is hampered by the lack of cellular and animal models on which to test
90 potentially effective therapies.
91 A main limitation in the development of CUP models is posed by the reduced availability of fresh
92 tumor cells, given that the biopsy is frequently entirely dedicated to the diagnostic workup and
93 surgery is rarely an option for these patients. Circulating tumor cells have been tracked in the blood
94 of CUP patients (10) and could be the source of tumor cells for cell lines development; this is true
95 also for ascites fluid, when available. Liquid biopsy tumor cells would have the advantage of being
96 more representative of the overall complexity and heterogeneity of CUP tumors.
97 Recently, Verginelli et al. described the generation of the first CUP *in vitro* and *in vivo* models from
98 biopsy/surgery tumor tissue, showing how they recapitulate the genetic of the original tumors and
99 present a stem cell-like phenotype (21). Since tumor cell proliferation in their models was sustained
100 by constitutively activation of the MAPK pathway, they described how the use of MEK1/2 inhibitor,
101 trametinib, strongly reduced cell viability and tumor volume in xenograft models. This is the first
102 study to describe the activation of an oncogenic pathway shared among CUPs, which supported a
103 specific therapeutic intervention.
104 In this study, we obtained and expanded two patient-derived CUP cell lines from ascites tumor cells,
105 spontaneously growing as spheroids and organoids, and corresponding patient-derived xenografts
106 (PDXs). We obtained the immunophenotypic, molecular and genomic characterization of the tumor
107 and derived models, confirming the recapitulation of the original features. Finally, we performed a
108 drug-screening assay to target actionable genes and identified a combination of drugs with promising
109 antitumor activity, both *in vitro* and *in vivo*.
110

111 **RESULTS**

112 **Establishment of two CUP models from ascites tumor cells: immunophenotypical, genetic and**
113 **molecular characterization**

114 We generated *in vitro* and *in vivo* CUP models to test tailored experimental pharmacological
115 approaches. CUP patient #55 was diagnosed with multiple lymph node metastases of poorly
116 differentiated adenocarcinoma. Immunohistochemistry (IHC) staining reported the positivity for
117 keratin 7 (K7) and CDX2, weak positivity for keratin 20 (K20) and negativity for neuroendocrine
118 markers (chromogranin, synaptophysin, CD56). CUP patient #96 presented with multiple metastases
119 of poorly differentiated adenocarcinoma with peritoneal carcinosis and multiple sub- and supra-
120 diaphragmatic lymph node metastases. The tumor IHC staining was positive for K7, K20, CDX2,
121 EpCAM and negative for PAX8, p40, GATA3 and calretinin.

122 Two long-term (more than 10 passages (22)) cell lines were obtained isolating cells from ascites fluid
123 of the patients #55 and #96. One month after seeding, cells growing in suspension were visible as
124 spheroid-like structures (**Figure S1**). The growth curve of two models was monitored for 10 days
125 using the Incucyte S3 live-cell analysis: 10000 cells of CUP#96 and CUP#55 were seeded and after
126 few hours CUP#96 cells formed large tumoroids and CUP#55 cells organized as clusters, showing a
127 doubling time of 5 days for both cell lines (**Figure S2 and S3**).

128 We generated two PDX models by injecting ascites tumor cells in the interscapular region of
129 immunocompromised mice as described in the Methods section. The two models showed different
130 growth rate, with CUP#96 PDX growing faster than CUP#55 PDX, and with CUP#55 PDX inducing
131 a tumor-intrinsic mild cachexia in the mice (**Figure S4**).

132 Morphology and histology of the cell lines and PDXs recapitulated the features of the primary tumor
133 (**Figure 1A-B**). To verify whether CUP tumor cells presented a stem-cell like phenotype, the two
134 tumoroid cell lines were tested for CD44 and EPCAM immunoreactivity and the expression of
135 stemness genes CD44, NANOG and OCT4/POU5F1 (**Figure 2**). The two cell lines express CD44 on
136 their surface, which is more homogeneous for CUP#96 (**Figure 2A**), and both express stemness genes
137 at high levels if compared to a panel of cancer cell lines (**Figure 2B**).

138 We recently developed a predictive microRNA-based test to assign a possible primary site to
139 metastatic cancers, including occult primary tumors (11). When we applied the predictive algorithms
140 to the two tumors, we obtained a site-of-origin prediction: CUP#55 was predicted to be of biliary
141 tract origin (probability of 93%) and CUP#96 of gastrointestinal tract origin (probability of 99%).
142 The tumor tissue, circulating cell-free DNA (ccfDNA), cell line and PDX were tested for genetic
143 alterations with a CUP-dedicated, 92-gene custom panel using SureSelect Target Enrichment
144 technology (Agilent Technologies) as described in (10). The summary of all genetic alterations is
145 reported in **Table 1** and **Table 2**. The genetic analysis of CUP#55 confirmed the detection of 5 genetic
146 alterations in all the analyzed samples (bulk tumor DNA, ccfDNA, cell line and PDX): the insertion
147 in the *APC* gene (p.T1556fs*3) and the point mutations in *ARID1A* (p.R1276∗), *ERBB3* (p.S128R),
148 *KEAP1* (p.R135H) and *NTRK1* (p.Q736X). Mutations in ALK, EPHA5, FAT1, KMT2C, MGA,
149 PTPRD (except for p.L970V) and TP53 were detected only in ccfDNA (**Table 1**). As expected, the
150 variant allele fractions (VAFs) were higher in PDX and cell line, thus reflecting the greater tumor
151 purity and the possible selection of tumor subclones. Low frequency mutations in *ZFHX3, RBM10,*
152 *PTPRT, NF1, MED12, MGA, KDR, KDM5A, GRIN2A, EP300, DOT1L, APC* (p. S887R), were
153 identified in the models but not in other samples. The generic analysis of CUP#96 was conducted on
154 ccfDNA and cell line due to the unavailability of residual tumor sample for this patient. Five genetic
155 alterations were detected in both samples (**Table 2**), with higher VAFs in the cell line compared to
156 ccfDNA. Low-pass Copy Number Analysis on the two cell lines revealed several regions of
157 amplification and deletion, including a >10 copies amplification in chromosome 10 encompassing
158 *FGFR2* oncogene (**Tables S1** and **S2**).
159

160 **Cell type identification using single cell transcriptomics**

161 Single-cell (sc) gene expression profiles of CUP#55 cell line were clustered on the basis of their
162 reciprocal similarity, leading to the identification of two separate clusters (**Figure 3A**). Automated

163 cell type annotation using the scType method identified the liver as the most likely tissue of origin
164 (**Figure 3B**).
165 We then applied a mapping approach using an atlas of liver cells as a reference, with the objective of
166 inferring the most likely type of origin for CUP cells in each cluster. While 93% of cells in cluster 1
167 were annotated as cholangiocytes (**Figure S5A**), the classification of cluster 2 was more diverse:
168 specifically, mapped types were split between cholangiocytes (73% of cells) and T/NK cells (27%).
169 As this separation did not correspond to any difference in cell morphology, we double-checked the
170 association manually. We identified the marker genes for the T/NK subgroup (**Supplemental**
171 **Material file S1**). This list is notable for two reasons: most of the genes are implicated in the cell
172 cycle, and in particular with the mitotic phase and DNA repair, as demonstrated by the results of
173 Metacore pathway enrichment analysis (**Figure 3C**). Furthermore, the list lacks any of the markers
174 which characterize the T/NK group in the liver atlas (CCL5, KLRB1, NKG7, CD69, GZMA, CCL4,
175 CST7, GNLY, GZMK). None of the cells in cluster 2 expresses any of those genes. This suggests
176 that the identification of T/NK cells by reference mapping is likely incorrect and driven by the
177 confounding effect of the cell cycle (**Figure S5B**). Indeed, an average of 46% of the cells in the
178 reference atlas are actively cycling, but when we focus on T/NK cells alone the percentage rises to
179 74%.
180

181 **Expression profiles of cell clusters**

182 The transcriptome analysis highlighted the presence of two separate cell clusters (**Figure 3A**),
183 labelled cluster 1 and cluster 2, with significant differences in their expression profiles. We identified
184 two sets of positive marker genes which characterize each cluster. Specifically, we obtained a total
185 of 1051 markers for the cluster 1 and 3059 for the cluster 2 (**Supplemental Material file S2**).
186 Functional annotation with Metacore of the markers for cluster 1 highlighted an over-representation
187 for pathways including Antigen presentation, Cytoskeleton remodeling and Cell adhesion (**Figure**

188 **S6**). A similar analysis of cluster 2 markers identified the following enriched pathways: regulation of
189 Wnt/beta-catenin pathway, VEGFR2 signaling and Double-strand break repair.
190 The sc gene expression analysis confirms the abundant expression of FGFR2 transcript and the
191 variable expression of genes markers of EMT and stemness (**Figure 4**), with SNAI1 and TGFB1
192 more expressed in cells belonging to cluster 1, and CD44, ZEB1 and HIF1A in cells of cluster 2.
193

194 **FGFR2 amplification in CUP#55 and CUP#96 cell lines provides the rationale to target the**
195 **receptor using a selective inhibitor**

196 FGFR2 genomic alterations are detected in CUPs with a frequency ranging from 3-4% (**Figure S7**).
197 The *FGFR2* amplification in our two models was confirmed with Fluorescence In Situ Hybridization
198 (FISH) and droplet digital PCR (ddPCR). FISH demonstrated the different nature of *FGFR2*
199 amplification: CUP#96 displays an extrachromosomal DNA amplification in the form of double
200 minutes; CUP#55 shows a homogeneously staining region (HSR) associated with *FGFR2*
201 chromosomal amplification (**Figure 5A**). The copy number variation (CNV) of *FGFR2* gene was
202 confirmed by ddPCR using a probe-based assay in circulating cell-free (ccfDNA), cell line and PDX
203 of both patients (**Figure 5B**). *FGFR2* copy number (CN) in tumor DNA is about 90 for CUP#55, and
204 >400 for CUP#96.
205 Consistent with the CN amplification, FGFR2 gene expression is increased in both cell lines (**Figure**
206 **5C**). We monitored the FGFR2 isoform expressed by the cell lines and found that both cell lines
207 express the epithelial FGFR2 IIIb isoform and the mesenchymal FGFR2 IIIc isoform (**Figure S8**).
208 Western blot analysis confirmed that CUP#96 cells express higher levels of total FGFR2 protein
209 compared to CUP#55 cells. Interestingly, in both models the FGFR2 appears constitutively
210 phosphorylated (**Figure 5D**). Notably, the FGFR2 phosphorylation/expression is higher than in a
211 reference FGFR2 positive cell line (H1581), derived from a lung adenocarcinoma with FGFR1 and
212 FGFR2 amplification (23) (**Figure 5C-D**). FGFR2 gene amplification and activation in CUP#55 and

213 CUP#96 cells provided the rationale for the pharmacological targeting of this receptor for therapeutic
214 intervention.
215
216 **Simultaneous inhibition of FGFR2/AKT and MAPK pathways by BGJ398 and trametinib,**
217 **respectively, induces synergistic anti-proliferative and pro-apoptotic effects in CUP models *in***
218 ***vitro***
219 We preliminarily tested a panel of multikinase inhibitors (BJ398, dovitinib, ponatinib) for their effect
220 on CUP#55 cell vitality. We selected BGJ398 (infigratinib), a selective inhibitor of the FGFR family,
221 for its greater antitumor activity (**Figure S9**) for further testing in CUP#55 and CUP#96 cells. In
222 CUP#55, the treatment with this drug at different concentrations (range 0.5-2.5 μM) inhibited FGFR2
223 phosphorylation and the downstream AKT/mTOR/p70S6K signaling (**Figure 6A**). In contrast,
224 ERK1/2 remained phosphorylated even at the highest BGJ398 concentration. CUP#55 cells were
225 sensitive to BGJ398 treatment, although a complete inhibition of their viability/proliferation was not
226 achieved even at 1 μM BGJ398 concentration, suggesting that FGFR-independent mechanisms
227 sustain the activation of the MAPK pathway and contribute to cell growth in this model. These results
228 prompted us to test whether targeting the MAPK pathway with trametinib, a highly specific inhibitor
229 of MEK1/2 proteins, might improve the efficacy of BGJ398 treatment. The drug combination
230 inhibited both the AKT and MAPK pathways almost completely (**Figure 6B**), thereby evidencing a
231 highly significant synergistic inhibition of cell proliferation, as indicated by the comparison with the
232 theoretical interaction curve in the Bliss experimental model ($p<0.001$) (**Figure 6C**). Interestingly,
233 even if the single treatment with either BGJ398 or trametinib did not induce cell death in CUP#55
234 cells, their combination had a cytotoxic effect, as demonstrated by fluorescence microscopy analysis
235 of Hoechst 33342/PI-stained cells; the morphology of the stained nuclei suggested that the cells died
236 by apoptosis (**Figure 6D, Figure S10**).
237 Then, we analyzed the effects of FGFR2 inhibition by BGJ398 treatment in CUP#96 cells. Inhibition
238 of FGFR2 phosphorylation by BGJ398 treatment resulted in the downregulation of phosphorylated

239 forms of AKT, p70S6K, and ERK1/2 levels, suggesting that both AKT and MAPK pathways are
240 downstream of FGFR2 in this cell model (**Figure 7A**). We tested the combination of BGJ398 with
241 trametinib also in these cells and found that it produced a remarkable synergistic inhibition of cell
242 proliferation (**Figure 7B-C**), comparable to that observed in CUP#55 cells, suggesting that trametinib
243 can provide a more effective inhibition of the MAPK pathway leading to suppression of cell growth
244 also in this cell model. Of note, BGJ398 and trametinib alone were cytotoxic in CUP#96 cells, an
245 effect that was further enhanced by the combined treatment (**Figure 7D**). Altogether, these findings
246 indicate that trametinib significantly improves the efficacy of FGFR2 targeting in FGFR2-amplified
247 CUP cells.
248
249 ***In vivo* synergic activity of FGFR2 and MEK inhibitors**
250 We tested whether *in vitro* findings on FGFR2 and MEK inhibitors synergic activity could be
251 recapitulated in CUP#55 and CUP#96 PDX models *in vivo*.
252 Mice were treated with control vehicle, BGJ398 (15 mg/kg), trametinib (0.6 mg/kg), and
253 trametinib/BGJ398 combination (N=5 per group). The scheme of different treatments is reported in
254 Figure 8 A and B, and the effect of different drugs was evaluated measuring the tumor volume. Single
255 drug (BGJ398 or trametinib) treatment significantly reduced the tumor volume in PDX#96 but not in
256 PDX#55 xenografts mice if compared to tumors of mice treated with vehicle. However, the
257 combination of trametinib and BGJ398 resulted more effective than the single treatments in both
258 PDX models, as demonstrated by the dramatic reduction of the tumor volume (**Figure 8A, B**).
259 CUP#55 PDX mice suffered from tumor-induced cachexia and for this reason they were sacrificed
260 after 2 weeks of treatment. CUP#96 PDX mice were treated for up to 33 days with the combination
261 and were sacrificed at 6 weeks.
262
263 **Transcriptome shift induced by treatment**

264 We analyzed the early effects of the combined treatment with MEK and FGFR2 inhibitors on
265 CUP#55 transcriptome at the single cell level. The treatment had a strong effect on the transcriptional
266 activity of the two cell clusters: we identified 526 and 2947 differentially expressed genes between
267 the treated and untreated cells, respectively in cluster 1 and 2 (**Supplemental Material file S3**). A
268 gene set enrichment analysis confirmed that the epithelial-mesenchymal transition was influenced by
269 the treatment, although at different degrees in the two clusters. Specifically, the signature identified
270 by Tuan *et al* (24) was the most enriched in cluster 1 (NES -2.36, adjusted p-value $7.81E^{-4}$), while
271 the signature from Cursons *et al* (25) was the most significant in cluster 2 (NES -3.09, adjusted p-
272 value $3.56E^{-8}$). The negative sign in both enrichment scores corresponds to an overall downregulation
273 of genes promoting the epithelial phenotype, suggesting a greater impact of the treatment on cells
274 with an epithelial phenotype.
275 Lastly, we extended our enrichment analysis to all signatures part of msigdb (**Supplemental Material**
276 **file S4**). We found the signature "ANDERSEN_CHOLANGIOCARCINOMA_CLASS2", which
277 collects genes overexpressed in cholangiocarcinoma class 2 associated with a poor prognosis, as
278 negatively enriched in cluster 2 (NES -3.34, adjusted p-value $8.53E^{-10}$). While the enrichment was
279 not significant in cluster 1 (adjusted p-value 0.02), the sign of the normalized enrichment score
280 remained negative (-2.2). Similarly, "HOSHIDA_LIVER_CANCER_SUBCLASS_S1" (genes from
281 'subtype S1' signature of hepatocellular carcinoma, linked to an aberrant activation of the WNT
282 signaling pathway) was enriched with a negative score in cluster 1 (NES -2.4, adjusted p-value $6.1E^{-}$
283 ^{3}), and obtained a negative but not significant score in cluster 2 (NES -2.1, adjusted p-value 0.02).
284 Overall, these results hint at a role of the treatment in reducing the activity of genes involved with
285 cancer progression.
286

287 **DISCUSSION**

288 Treatment choice for cancer of unknown primary patients is always challenging due to the
289 inconclusiveness of classical diagnostic investigations in tumor type identification. In this scenario,

290 therapy can be based on empirical approaches, molecular predictions of the primary site, the clinical
291 assessment of the similarity with other known tumor types or more recently, on personalized genetic
292 approaches. Indeed, the combination of molecular and genetic investigations can help the treating
293 clinicians to define the most probable site-of-origin or potential druggable mutations and use this
294 information to choose the best therapeutic strategies.
295 CUP therapeutic choice has been also hampered by the lack of CUP models on which to test novel
296 therapeutic approaches or investigate the biology of this aggressive disease. Verginelli et al. described
297 the first CUP experimental models adopted to investigate molecular and genetic alterations of the
298 disease (21). The authors demonstrated that CUP models present a specific stem-cell like phenotype
299 and tested for the first time their sensitivity to MEK inhibitors. Here, we described two *in vitro* and
300 *in vivo* models we derived from ascites circulating tumors cells (CTCs) of CUP patients, named
301 CUP#55 and CUP#96. Using a CTC-optimized protocol, we established two long-term cell cultures
302 spontaneously growing as spheroids/tumoroids and expressing stem-cell markers. Combined
303 investigations on microRNA expression, single cell transcriptomics and genomic alterations pointed
304 toward a biliary tract origin for CUP#55 and gastrointestinal origin for CUP#96.
305 The ascites CTCs were engrafted into mice to generate two patients derived xenografts, which
306 recapitulated the characteristics of the original tumor. The genetic analyses, performed on tumor
307 tissues and models, revealed that the two models shared the FGFR2 amplification as main genetic
308 alteration, although of a different nature. FGFR2 amplification is reported in several solid tumors,
309 including gastric cancer and breast cancer (26), while its translocation is a recurrent feature in
310 cholangiocarcinoma (27).
311 FGFR2 amplification is associated with increased levels of the protein and its aberrant
312 phosphorylation leads to the activation of downstream pathways, including MAPK-ERK signaling
313 (28), which in turn accelerate cell proliferation. Since FGFR2 amplification is a druggable target (28)
314 we investigated the extent of CUP tumors FGFR2 dependency. The treatment with BGJ398
315 (infigratinib), a pan-FGFR inhibitor, demonstrated the effectiveness of this target therapy in reducing

316 AKT activation, but did not completely prevent ERK1/2 phosphorylation, which remained active
317 through alternative mechanisms. This finding suggests that FGFR2 targeting in FGFR2-amplified
318 CUPs might not be sufficient to halt tumor growth, due to the concomitant activation of alternative
319 survival/proliferation pathways. Therefore, we investigated the effect of the combined use of
320 trametinib, a MAPK pathway inhibitor selective for MEK1/2. MAPK is a pathway that is frequently
321 activated in CUPs (29), where its activation correlates with worse prognosis. Interestingly, the
322 combined treatment with FGFR2 and MEK inhibitors generated a remarkable synergistic effect,
323 reducing cell growth and viability in both cell models with induction of cell death.
324 The short-term combined treatment of cultured cells revealed a degree of plasticity in the apparently
325 homogeneous cell line, which could be evidenced only from single-cell transcriptomic data. The
326 transformed cholangiocytes of CUP#55 cell line were differentially affected by the combined
327 treatment, with genes involved in cancer progression being silenced in both cell subgroups (clusters)
328 and cells expressing an epithelial phenotype being more susceptible to treatment-induced cell death.
329 To validate the results in a preclinical model, the corresponding PDXs were treated with the drug
330 combination and the effect was a drastic reduction of the tumor size if compared with single
331 treatments. The treatment combination was well tolerated by the CUP#96 model but aggravated the
332 mice frailty in CUP#55 model, which already presented signed of tumor-induced cachexia.
333 In the last years, pemigatinib and infigratinib, both orally active agents targeting FGFR1-4, have
334 received an accelerated approval by US Food and Drug Administration (FDA) for the treatment of
335 adult patients with previously treated and unresectable or metastatic cholangiocarcinoma harboring
336 FGFR2 fusion or other rearrangement. Based on some concerns, European agency (EMA) granted
337 approval with the same indication only for pemigatinib. Likewise, erdafitinib, an orally active small
338 potent TKI of FGFR1–4, was granted accelerated approval for patients with locally advanced or
339 metastatic urothelial carcinoma, with susceptible FGFR3 or FGFR2 genetic alterations.
340 FGFR inhibitors have also been largely tested in gastric cancer patients with less enthusiastic results
341 so far. However, positive results from a phase II trial have been reported by using bemarituzumab in

342 addition to chemotherapy as first line treatment for metastatic HER-2 negative gastroesophageal
343 cancer patients with FGFR2b hyperexpression or FGFR2 gene amplification (30). As such, several
344 phase II and phase III trials currently ongoing. Other new compounds, alone or in combination with
345 other agents, are under investigation for the treatment of multiple solid tumors carrying FGFR
346 alterations. Our results suggest that the combination of FGFR and MEK inhibitors could be a potential
347 strategy to improve clinical outcomes in cancer patients carrying FGFR gene alterations. This means
348 that co-targeting cross-talking pathways may potentiate FGFR inhibition, and improve the therapeutic
349 benefit, as we have demonstrated with the MEK inhibitor trametinib.
350 Based on the evidence that MEK inhibition in KRAS-mutant lung cancer leads to compensatory
351 MAPK pathway reactivation through FGFR1, combining trametinib with FGFR1-specific inhibitors
352 encapsulated in nanoparticles allowed to efficaciously inhibit growth and proliferation in KRAS-
353 mutant/FGFR compensatory cancer cells (31). In this regard, a phase 1/2 study is recruiting patients
354 with advanced cancer of any tumor type (Part 1) or non-small cell lung cancer (NSCLC) with a
355 confirmed KRAS mutation (Part 2) aiming at determining the recommended dose and antitumor
356 activity of futibatinib (a selective, irreversible FGFR1-4 inhibitor) in combination with binimetinib,
357 a known MEK inhibitor (NCT04965818).
358 Our study contributes to fill the gap in CUP model availability, through the generation of two human
359 cell lines and corresponding PDXs. We demonstrated how the molecular characterization and genetic
360 profile of the tumor can provide information to predict the most probable site-of-origin and identify
361 druggable targets. In fact, the development of models that mirror the phenotype and genotype of
362 human tumors *in vitro* and *in vivo*, has become a helpful tool for drug screening, particularly to assess
363 new therapeutic combinations that could be translated to patients with the same genetic alterations or
364 molecular features. Finally, the availability of CUP models for future studies will contribute to deepen
365 our knowledge on the mechanisms at the base of CUP high proliferative and metastatic potential and
366 still mysterious biology.
367

368 **MATERIALS AND METHODS**

369 **Study approval**

370 Two patients with a confirmed diagnosis of cancer of unknown primary based on ESMO criteria
371 (CUP#55 and CUP#96) were enrolled in this study at the Oncology Unit of IRCCS Azienda
372 Ospedaliero-Universitaria di Bologna (Bologna, Italy). The study was approved by the local ethical
373 committee (Comitato Etico Indipendente dell'Azienda Ospedaliero-Universitaria di Bologna,
374 Policlinico S.Orsola Malpighi) with protocol number EM435-2022_130/2016/U/Tess/AOUBo. All
375 subjects provided a written informed consent to the study participation, in accordance with the
376 Declaration of Helsinki.

377

378 **Cell culture**

379 NSCLC cell lines H1581, A549, H460, H2228, H1299 and SK-MEL-28 were from ATCC (Manassas,
380 VA, USA).

381 Cells were cultured in RPMI-1640 medium (Corning) supplemented with 10% fetal bovine serum
382 (Corning) and maintained under standard cell culture conditions at 37°C in a water-saturated
383 atmosphere of 5% CO_2 in air.

384

385 **Patients and ascites CTC isolation**

386 About 100 ml of ascites from both patients were collected and immediately processed. Ascites
387 samples were centrifuged at 600 g for 10 minutes at 4°C and the obtained pellet was treated with 10
388 ml red blood cell lysis buffer (Miltenyi Biotec) for 15 minutes at room temperature. Then, 10 ml of
389 specific culture medium (DMEM/F12 50:50, 2 mM glutamine, 5% Horse serum, hydrocortisone 1
390 ug/ml, insuline 10 µg/ml, 1X PEN/STREP, EGF 10 ng/ml) was added and centrifuged at 600 g for
391 10 minutes. The cells were plated in T25 flask with 5 ml of medium in humidified 37 °C/5% CO_2
392 incubator. Medium was changed every 3–4 days. After 10 days, tumor cells begun to grow as
393 tumoroids (CUP#96) and spheroids (CUP#55).

394 Organoids and aggregates were propagated in 24 well-plates to monitor growth and every 3-4 days
395 splitted 1:2. Long-term CTC cell lines were established: i.e. the cell lines were still viable after
396 thawing cycle and showed a stable growth in medium without supplement (32).
397

398 **Pathological and immunofluorescence analysis**

399 Cell lines, human and PDX tumor tissues were fixed in 4% paraformaldehyde for 20 minutes,
400 embedded in paraffin and frozen at -20°C for optimal cutting. Sections of 4 µm were mounted on
401 positively charged microscope slides. Sections were deparaffinized in xylene and rehydrated in
402 graded alcohol. Antigen enhancement was done by incubating the sections in Concentrated Antigen
403 Retrival Solution Citra Plus (BioGenex #HK080-5K) (1:10) as recommended by the manufacturer
404 and blocked with Ventana Antibody Diluent with Casein (Roche-Ventana) for 30 minutes. For
405 immunohistochemistry: Rabbit Monoclonal Primary Antibody Cytokeratin 7 (SP52) (Roche-
406 Ventana) and Rabbit Monoclonal Primary Antibody Cytokeratin 20 (SP33) (Roche-Ventana), were
407 used at 1:2 dilution for cell lines, human and PDX tumor tissues staining.
408 For immunofluorescence experiment: Mouse Monoclonal Primary Antibody CD44 (or HCAM) sc-
409 7297 (SantaCruz) 1:100 dilution and Mouse Monoclonal Primary Antibody EpCAM FITC (REA764)
410 (Miltenyi) 1:100 dilution was used for cell lines staining. All the antibodies were incubated overnight
411 at 4°C. AbCAM Goat Anti-Rabbit IgG H&L (DyLight® 594) (ab96885) and Donkey Anti-Mouse
412 IgG H&L (DyLight® 488) (ab96875) labeled secondary antibodies were used at 1:100 dilution and
413 incubated 1h. Nuclei were counterstained with 1 µg/mL of Hoechst 33342 (Life Technologies).
414 Confocal images were acquired on Nikon A1 confocal laser scanning microscope, equipped with a
415 60X, 1.4 NA objective and with 405, 488 nm laser lines.
416

417 **Genetic analysis**

418 We used a custom 1.2-Mb SureSelect capture bait library (Agilent Technologies, Santa Clara, CA,
419 United States) for the target enrichment of 92 genes (panel description in (Laprovitera et al., 2021c)).

420 Briefly, libraries were prepared using 50 ng of gDNA input following SureSelectXT
421 HS/SureSelectXT Low Input Target Enrichment with Pre-Capture Pooling protocol (G9702-90005,
422 v. A0, June 2019, Agilent Technologies) and sequenced on NextSeq 500 (Illumina) platform using
423 High Output 2 × 75-bp flow cells. Variant calling and paired analyses (tumor vs. normal) were
424 performed using SureCall software (v. 4.2), applying a filter for tumor/normal tissue/models at 5%
425 and for ccfDNA at 1%. Variants were annotated using ANNOVAR (Wang et al., 2010) and filtered
426 to keep somatic exonic non-synonymous single-nucleotide variants (SNVs), insertions, deletions,
427 multiple nucleotide variants, or long deletions not detected in the normal sample that presented an
428 allele frequency in Non-Finnish European (NFE) population lower than 0.5% (Genome Aggregation
429 Database, GnomAD; Karczewski et al., 2020) and a coverage higher than 100. Bioinformatic
430 pathogenicity prediction, reported in Tables 1 and 2 of the identified variants was performed
431 consulting the prediction score/outcome of 8 prediction models: SIFT (Sort Intolerated From
432 Tolerated; Vaser et al., 2016), Polyphen2 HVAR (Polymorphism Phenotyping v2; Adzhubei et al.,
433 2010), LRT (Likelihood Ratio Test; Chun and Fay, 2009), Mutation Taster (Schwarz et al., 2014),
434 Mutation Assessor (Reva et al., 2011), FATHMM (Functional Analysis Through Hidden Markov
435 Model; Shihab et al., 2013), CADD (Combined Annotation Dependent Depletion; Kircher et al.,
436 2014), and VEST (Variant Effect Scoring Tool; Douville et al., 2016). Variants were considered
437 pathogenic when more than 50% of the above-mentioned predictors indicated it as
438 pathogenic/damaging/deleterious/harmful.
439

440 **Single cell transcriptome analysis**

441 The transcriptome of CUP#55 cell line was characterized at the single-cell level. To this end, we
442 relied on the 10X Single Cell 5' R2-only kit. The resulting libraries were sequenced with the Novaseq
443 6000 (Illumina) platform using a 2 × 100-bp flow cell, obtaining a total yield of 240 million reads.
444 Gene expression profiles of different cells were quantified by the CellRanger pipeline (version 7.1.0),
445 using as a reference the GENCODE annotation (version 40). The software provided an initial estimate

446 of 23,994 sampled cells. Gene counts were filtered by means of the CellBender method (33) to
447 remove the confounding effects of ambient RNA molecules and random barcode swapping. Around
448 7% of all droplets were identified by scDblFinder (34) (version 1.14.0) as potential doublet artifacts
449 and were excluded from the rest of the analysis. We also discarded cells characterized by a high
450 proportion of reads from the mitochondrial genome, a signal usually associated with cell membrane
451 rupture and apoptosis. We set our filtering threshold to 50% following the indications of other studies
452 (35) that have observed very high mitochondrial content in hepatocytes. As a last QC filter, we
453 dropped all cells showing a detectable level of expression for less than 500 genes. The final working
454 set consisted of 1437 cells.
455 Gene expression was loaded in the R environment using Seurat (36) (version 4.3.0.1) and normalized
456 with the sctransform (37) method (v2) to account for gene overdispersion. Cells were clustered using
457 the Latent Cellular Analysis method (38) (scLCA package, version 0.0.0.9000), which combines a
458 cosine-similarity measure with a graph-based algorithm to automatically identify distinct cell
459 subpopulations. Automatic inference of the tissue type was performed with scType
460 (https://doi.org/10.1038/s41467-022-28803-w) (version 1.0). Reference-based classification of cells
461 was then performed using the Azimuth software (36) (version 0.4.6) and relied on its integrated atlas
462 of the human liver..
463 We applied the MAST software (39) to identify marker genes of cell clusters. This method (version
464 1.24.0) implements a generalized linear model specifically designed to account for nuisance variation
465 in scRNA-seq data. We filtered differential expression calls by setting an FDR threshold of 10^{-3}, and
466 we also discarded all genes whose log2 fold-change lied below 0.2.
467 Functional analysis of the resulting gene lists was performed using MetaCore analytical software
468 (Clarivate).
469
470 **Gene expression analysis**

471 RNA was extracted from 2 CUP cell lines and 5 cancer cell lines (A549, H2228, H460, H1299,
472 SKMEL). 500ng of RNA for each cell line were reverse-transcribed to cDNA using iSRCIPT cDNA
473 Synthesis Kit (Cat. No. 1708891 Bio-Rad, USA). The expression of CD44, NANOG, OCT4, and
474 FGFR2 was quantified using the QX200 Droplet Digital PCR system (Bio-Rad, Hercules, CA, USA).
475 Bio-Rad EvaGreen protocol for gene expression quantification was used to quantify the gene copies
476 per ng of cDNA by QuantaSoft Analysis software (Bio-Rad, Hercules, CA, USA). Gene/HPRT
477 (reference gene) ratio was used to normalize the gene expression. The primers used for the gene
478 expression analysis are reported in supplementary material.
479

480 **Fluorescence In-Situ Hybridization (FISH)**

481 FISH analysis was performed on fixed CUP#55 and CUP#96 interphase nuclei and metaphases. Two
482 Empire Genomics probes (Empire Genomics, Buffalo, NY) were employed following the
483 manufacturer's protocol. Specifically, the FGFR2 gene probe (orange) maps on chr:10q26.13 and the
484 CEP10 probe maps to the centromeric region of Chromosome 10. CUP#55 and CUP#96 cells were
485 counterstained with 40,6-diamidino-2-phenylindole (DAPI) for nuclear detection. Analysis was
486 performed using Olympus BX53 microscopy equipped with the appropriate filter sets and CytoVision
487 software (Leica Biosystems, Nussloch, Germany).
488

489 **Detection of *FGFR2* amplification**

490 Total DNA was extracted from CUP#55 and CUP#96 cell lines and PDXs using QIAamp DNA Mini
491 Kit (Cat. No. 5130450, Qiagen). Cell free DNA was extracted from 1mL plasma with Maxwell RSC
492 ccfDNA Plasma Kit (Cat No: AS1480, Promega). Tumor DNA was extracted using the QIAamp
493 DNA FFPE Tissue Kit (Cat No: 56404, Qiagen, Hilden, Germany). To quantify the copy number of
494 FGFR2 in all samples, a probe-based droplet digital PCR assay was used. RPP30 was tested as
495 reference gene for diploid copy number. RPP30 probe (dHsaCP2500350, Bio-Rad) was labeled with
496 HEX, and FGFR2 probe (dHsaCB2500320) was labeled with FAM. Droplet digital PCR was

497 performed with the QX200 Droplet Digital PCR system (Bio-Rad, USA) as described in (10). FGFR2
498 gene copy number was calculated by QuantaSoft Analysis software (Bio-Rad, Hercules, CA, USA)
499 as FGFR2/RPP30 ratio.
500
501 **Cell Viability and Drug response assays**
502 Cell viability/proliferation was evaluated by a CellTiter-Glo 96 Aqueous One solution Assay
503 (Promega). Cell death was analyzed by fluorescence microscopy after staining with Hoechst 3342
504 and Propidium Iodide (PI) (40). BGJ398 (infigratinib) and trametinib (mekinist) were purchased from
505 Selleckchem (Houston, TX), and dissolved in DMSO. DMSO concentration never exceeded 0.1%
506 (v/v); equal amounts of the solvent were added to control cells. The effect of the drug combination
507 was evaluated using the Bliss interaction model (41).
508
509 **Single cell transcriptome of treated cells**
510 We profiled the transcriptome of CUP#55 cells treated with MEK and FGFR2 inhibitors for 12 hours
511 using a single-cell protocol similar to the one discussed for the CUP#55 line. Illumina sequencing
512 resulted in 260 million reads, providing a reliable readout for 1789 cells after the application of quality
513 control filters. The shift in gene expression between treated and untreated cells was evaluated
514 separately for each cluster using MAST and setting an FDR cutoff of 10^{-6}.
515 We employed fgsea (version 1.24.0) (42) to perform a gene set enrichment analysis. Gene signatures
516 were retrieved using msigdb (Bhuva D, Smyth G, Garnham A (2022). _msigdb: An ExperimentHub
517 Package for the Molecular Signatures Database (MSigDB) 10.18129/B9.bioc.msigdb package
518 version 1.6.0, database version 7.5). We downloaded an additional collection of gene sets specifically
519 related to the epithelial-mesenchymal transition from the EMTome database (43) (data retrieved on
520 05/03/2023). We finally filtered fgsea results by placing an upper threshold of 10^{-2} on the Benjamini-
521 Hochberg adjusted p-values.
522

523 **Western blotting**

524 For Western Blot analysis, $8x10^5$ cells from CUP#55 or CUP#96 were seeded in 6 well-plates in
525 complete culture medium. At the end of the treatments, the cells were harvested and centrifuged. The
526 procedures for protein extraction, solubilization, and protein analysis by western blotting are
527 described elsewhere (44). Antibodies against p-FGFR (#3471), FGFR2 (#11835), p-
528 ERK1/2$^{Thr202/Tyr204}$ (#4370), ERK1/2 (#4695), p-AKT^{Ser473} (#9271), AKT (#9272), p-P70S6K^{Thr389}
529 (#9205), P70S6K (#9202) were from Cell Signaling Technology, Incorporated (Danvers, MA); anti-
530 β-actin (clone B11V08) was from BioVision (Milpitas, CA). Horseradish peroxidase-conjugated
531 secondary antibodies and the chemiluminescence system were from Millipore (Millipore, MA).
532 Reagents for electrophoresis and blotting analysis were from BIO-RAD Laboratories (Hercules, CA).
533 The chemiluminescent signal was acquired by C-DiGit R Blot Scanner and the bands were quantified
534 by Image StudioTMSoftware, LI-COR Biotechnology (Lincoln, NE).

535

536 **Growth of CUP tumors in immunocompromised mice**

537 PDX studies were run at XenTech in compliance with authorization n. APAFIS#30365-
538 2021012215599431 v1 conferred from the French Ministry of Agriculture and Food. The
539 authorization to use animals in the CERFE facility (Evry-Courcouronne, France) was obtained by
540 The Direction Départementale de la Protection des Populations, Ministère de l'Agriculture et de
541 l'Alimentation, France "Direction of the Veterinarian Services, Ministry of Agriculture and Food,
542 France" (agreement No. D-91-228-107).

543 An approximate number of 3-4000 cells or 30-40 organoids were resuspended in 100 µl of culture
544 medium, diluted 1:1 in matrigel and grafted in the interscapular region of NOD/Scid-IL2Rγ-/- (NSG)
545 or NOD/Shi-scid/IL-2Rγnull (NOG) mice. Tumor fragments were sampled from the resected tumor,
546 minced on ice and immediately placed in MACS Tissue Storage Solution (Miltenyi Biotech) and
547 transferred to the animal facility, fragmented and grafted in the interscapular region of Athymic
548 Nude-Foxn1nu mice. Mice were monitored twice weekly for signs of tumor growth. Tumor growth

549 from first implantation occurred in 135 days for CUP#55 and 40 days for CUP#96. Growing tumors
550 were serially transplanted onto recipient mice and the fragments of the tumor harvested for IHC
551 analysis, DNA and RNA extraction. To immortalize each PDX, vials of tumor fragments at different
552 passages were placed in 90% FCS/10% DMSO or glycerol, and stored at -150°C.
553

554 ***In vivo* treatments**

555 Treatment efficacy study on each PDX were run as follows. Tumor fragments of the same passage
556 were transplanted subcutaneously onto 3-24 mice (donor mice). When the tumors reached 700 to
557 1764 mm^3, donor mice were sacrificed, and tumors were cut into fragments measuring approximately
558 20 mm^3. Mice aged 8 to 11 weeks were anaesthetized with 100 mg/kg ketamine hydrochloride and
559 10 mg/kg xylazine, and one tumor fragment was placed in the interscapular fat pad. On the day of
560 enrollment in the study mice with tumor volume ranging 60 to 200 mm^3 were randomly attributed to
561 the different groups:
562

Gr.	N	1st Testing Agent					2nd Testing Agent				
		Agent	Dose mg/kg	Route	Volume ml/kg	Schedule	Agent	Dose mg/kg	Route	Volume ml/kg	Schedule
1	5	Vehicle 1	-	PO	10	qd	Vehicle 2	-	PO	10	qd
2	5	trametinib	0.6*	PO	10	qd	-	-	-	-	-
3	5	-	-	-	-	-	BGJ398	15*	PO	10	qd
4	5	trametinib	0.6	PO	10	qd	BGJ398	15	PO	10	qd

564 Legend: PO= per os; qd= once daily
565

566 From day 12 to day 14 half dose was administered due to body weight loss.
567 Trametinib was purchased at Carbosynth and suspended in 10% DMSO; 40% PEG300; 5% Tween-
568 80; 45% NaCl 0.9% for administration; BGJ398 (infigratinib) was purchased at MedChem Express
569 and diluted in 50% Acetic acid/acetate buffer / 50% PEG300 for administration. Tumor volume was
570 evaluated by measuring tumor diameters with a caliper, three times a week during the treatment

571 period (from D0 to D27); all animals were weighted, and tumor size measured the same day. During
572 the whole experimental period, animals were monitored every day for physical appearance, behavior,
573 and clinical changes.
574

575 **Data availability statement**

576 Processed single-cell transcriptomic data are available as supplementary information. MicroRNA,
577 genomic and single-cell transcriptomic raw data are available from the authors upon request.
578

579 **Acknowledgments**

580 The research leading to these results has received funding from Fondazione Italiana per la Ricerca
581 sul Cancro AIRC grant IG 2021 - ID. 25789 to Manuela Ferracin, Pallotti Institutional funds to
582 Manuela Ferracin, Fondazione del Monte to Manuela Ferracin, UNIPD PRID 2019 – ID.
583 BIRD193023 to Gabriele Sales.
584

585 **Author contributions:**

586 Conceptualization: AC, MF
587 Methodology: EP, SC, GS, AC
588 Investigation: AC, CF, IS, NL, GG, MR, MN, SS, EB, GD, RR
589 Funding Acquisition: MF
590 Resources: FG, KR, ML, IG, AD, OD, PGP, AA, GS and MF
591 Writing-Original Draft: AC, IS, CF, GS, MF
592 Writing-Review & Editing: GAC, MB, AA, GS, MF
593

594 **Declaration of interests**

Francesco Gelsomino received personal fees from AstraZeneca and honoraria for advisory board participation from Eli-Lilly. George Calin is a member of the Editorial Board of Molecular Therapy. All the other authors declare no competing interests.

Keywords

CUP, patient-derived xenografts, genetic test, FGFR2, FGFR2 inhibitor, MEK inhibitor, infigratinib, site-of-origin prediction

604 **References and Notes**

605

606 1. Chaffer CL, and Weinberg RA. A perspective on cancer cell metastasis. *Science.*
607 2011;331(6024):1559-64.
608 2. Varadhachary GR, and Raber MN. Cancer of unknown primary site. *N Engl J Med.*
609 2014;371(8):757-65.
610 3. Laprovitera N, Riefolo M, Ambrosini E, Klec C, Pichler M, and Ferracin M. Cancer of
611 Unknown Primary: Challenges and Progress in Clinical Management. *Cancers (Basel).*
612 2021;13(3).
613 4. Warner E, Goel R, Chang J, Chow W, Verma S, Dancey J, et al. A multicentre phase II
614 study of carboplatin and prolonged oral etoposide in the treatment of cancer of unknown
615 primary site (CUPS). *Br J Cancer.* 1998;77(12):2376-80.
616 5. Pentheroudakis G, Briasoulis E, Kalofonos HP, Fountzilas G, Economopoulos T, Samelis
617 G, et al. Docetaxel and carboplatin combination chemotherapy as outpatient palliative
618 therapy in carcinoma of unknown primary: a multicentre Hellenic Cooperative Oncology
619 Group phase II study. *Acta Oncol.* 2008;47(6):1148-55.
620 6. Briasoulis E, Fountzilas G, Bamias A, Dimopoulos MA, Xiros N, Aravantinos G, et al.
621 Multicenter phase-II trial of irinotecan plus oxaliplatin [IROX regimen] in patients with
622 poor-prognosis cancer of unknown primary: a hellenic cooperative oncology group study.
623 *Cancer Chemother Pharmacol.* 2008;62(2):277-84.
624 7. Huebner G, Link H, Kohne CH, Stahl M, Kretzschmar A, Steinbach S, et al. Paclitaxel and
625 carboplatin vs gemcitabine and vinorelbine in patients with adeno- or undifferentiated
626 carcinoma of unknown primary: a randomised prospective phase II trial. *Br J Cancer.*
627 2009;100(1):44-9.
628 8. Hainsworth JD, Spigel DR, Clark BL, Shipley D, Thompson DS, Farley C, et al.
629 Paclitaxel/carboplatin/etoposide versus gemcitabine/irinotecan in the first-line treatment of

630 patients with carcinoma of unknown primary site: a randomized, phase III Sarah Cannon
631 Oncology Research Consortium Trial. *Cancer J.* 2010;16(1):70-5.
632 9. Gross-Goupil M, Fourcade A, Blot E, Penel N, Negrier S, Culine S, et al. Cisplatin alone or
633 combined with gemcitabine in carcinomas of unknown primary: results of the randomised
634 GEFCAPI 02 trial. *Eur J Cancer.* 2012;48(5):721-7.
635 10. Laprovitera N, Salamon I, Gelsomino F, Porcellini E, Riefolo M, Garonzi M, et al. Genetic
636 Characterization of Cancer of Unknown Primary Using Liquid Biopsy Approaches. *Front*
637 *Cell Dev Biol.* 2021;9:666156.
638 11. Laprovitera N, Riefolo M, Porcellini E, Durante G, Garajova I, Vasuri F, et al. MicroRNA
639 expression profiling with a droplet digital PCR assay enables molecular diagnosis and
640 prognosis of cancers of unknown primary. *Mol Oncol.* 2021;15(10):2732-51.
641 12. Hayashi H, Takiguchi Y, Minami H, Akiyoshi K, Segawa Y, Ueda H, et al. Site-Specific
642 and Targeted Therapy Based on Molecular Profiling by Next-Generation Sequencing for
643 Cancer of Unknown Primary Site: A Nonrandomized Phase 2 Clinical Trial. *JAMA Oncol.*
644 2020;6(12):1931-8.
645 13. Clynick B, Dessauvagie B, Sterrett G, Harvey NT, Allcock RJN, Saunders C, et al. Genetic
646 characterisation of molecular targets in carcinoma of unknown primary. *J Transl Med.*
647 2018;16(1):185.
648 14. Ross JS, Wang K, Gay L, Otto GA, White E, Iwanik K, et al. Comprehensive Genomic
649 Profiling of Carcinoma of Unknown Primary Site: New Routes to Targeted Therapies.
650 *JAMA Oncol.* 2015;1(1):40-9.
651 15. Varghese AM, and Saltz LB. Genomic Profiling of Cancers of Unknown Primary Site: The
652 Next Steps. *JAMA Oncol.* 2015;1(4):541-2.
653 16. Zehir A, Benayed R, Shah RH, Syed A, Middha S, Kim HR, et al. Mutational landscape of
654 metastatic cancer revealed from prospective clinical sequencing of 10,000 patients. *Nat*
655 *Med.* 2017;23(6):703-13.

656 17. Consortium APG. AACR Project GENIE: Powering Precision Medicine through an
657 International Consortium. *Cancer Discov.* 2017;7(8):818-31.
658 18. Lombardo R, Tosi F, Nocerino A, Bencardino K, Gambi V, Ricotta R, et al. The Quest for
659 Improving Treatment of Cancer of Unknown Primary (CUP) Through Molecularly-Driven
660 Treatments: A Systematic Review. *Front Oncol.* 2020;10:533.
661 19. Gatalica Z, Xiu J, Swensen J, and Vranic S. Comprehensive analysis of cancers of unknown
662 primary for the biomarkers of response to immune checkpoint blockade therapy. *Eur J*
663 *Cancer.* 2018;94:179-86.
664 20. Ding Y, Jiang J, Xu J, Chen Y, Zheng Y, Jiang W, et al. Site-specific therapy in cancers of
665 unknown primary site: a systematic review and meta-analysis. *ESMO Open.*
666 2022;7(2):100407.
667 21. Verginelli F, Pisacane A, Gambardella G, D'Ambrosio A, Candiello E, Ferrio M, et al.
668 Cancer of unknown primary stem-like cells model multi-organ metastasis and unveil
669 liability to MEK inhibition. *Nat Commun.* 2021;12(1):2498.
670 22. Janik K, Popeda M, Peciak J, Rosiak K, Smolarz M, Treda C, et al. Efficient and simple
671 approach to in vitro culture of primary epithelial cancer cells. *Biosci Rep.* 2016;36(6).
672 23. SenthilKumar G, Fisher MM, Skiba JH, Miller MC, Brennan SR, Kaushik S, et al. FGFR
673 Inhibition Enhances Sensitivity to Radiation in Non-Small Cell Lung Cancer. *Mol Cancer*
674 *Ther.* 2020;19(6):1255-65.
675 24. Tan TZ, Miow QH, Miki Y, Noda T, Mori S, Huang RY, et al. Epithelial-mesenchymal
676 transition spectrum quantification and its efficacy in deciphering survival and drug
677 responses of cancer patients. *EMBO Mol Med.* 2014;6(10):1279-93.
678 25. Cursons J, Leuchowius KJ, Waltham M, Tomaskovic-Crook E, Foroutan M, Bracken CP, et
679 al. Stimulus-dependent differences in signalling regulate epithelial-mesenchymal plasticity
680 and change the effects of drugs in breast cancer cell lines. *Cell Commun Signal.* 2015;13:26.

681 26. Katoh M. Cancer genomics and genetics of FGFR2 (Review). *Int J Oncol.* 2008;33(2):233-
682 7.
683 27. Smyth EC, Babina IS, and Turner NC. Gatekeeper Mutations and Intratumoral
684 Heterogeneity in FGFR2-Translocated Cholangiocarcinoma. *Cancer Discov.* 2017;7(3):248-
685 9.
686 28. Babina IS, and Turner NC. Advances and challenges in targeting FGFR signalling in cancer.
687 *Nat Rev Cancer.* 2017;17(5):318-32.
688 29. Krikelis D, Pentheroudakis G, Goussia A, Siozopoulou V, Bobos M, Petrakis D, et al.
689 Profiling immunohistochemical expression of NOTCH1-3, JAGGED1, cMET, and
690 phospho-MAPK in 100 carcinomas of unknown primary. *Clin Exp Metastasis.*
691 2012;29(6):603-14.
692 30. Wainberg ZA, Enzinger PC, Kang YK, Qin S, Yamaguchi K, Kim IH, et al. Bemarituzumab
693 in patients with FGFR2b-selected gastric or gastro-oesophageal junction adenocarcinoma
694 (FIGHT): a randomised, double-blind, placebo-controlled, phase 2 study. *Lancet Oncol.*
695 2022;23(11):1430-40.
696 31. Izawa-Ishiguro AR, Sridharan R, Wun C, Sami TJ, and Heller DA. Abstract 302: MEKi-
697 FGFRi combination nanoparticles for use against KRASmt/FGFR-compensatory lung
698 tumors. *Cancer Research.* 2022;82(12_Supplement):302-.
699 32. Kodack DP, Farago AF, Dastur A, Held MA, Dardaei L, Friboulet L, et al. Primary Patient-
700 Derived Cancer Cells and Their Potential for Personalized Cancer Patient Care. *Cell Rep.*
701 2017;21(11):3298-309.
702 33. Fleming SJ, Chaffin MD, Arduini A, Akkad AD, Banks E, Marioni JC, et al. Unsupervised
703 removal of systematic background noise from droplet-based single-cell experiments using
704 CellBender. *Nat Methods.* 2023;20(9):1323-35.
705 34. Germain PL, Lun A, Garcia Meixide C, Macnair W, and Robinson MD. Doublet
706 identification in single-cell sequencing data using scDblFinder. *F1000Res.* 2021;10:979.

707 35. MacParland SA, Liu JC, Ma XZ, Innes BT, Bartczak AM, Gage BK, et al. Single cell RNA
708 sequencing of human liver reveals distinct intrahepatic macrophage populations. *Nat*
709 *Commun.* 2018;9(1):4383.
710 36. Hao Y, Hao S, Andersen-Nissen E, Mauck WM, 3rd, Zheng S, Butler A, et al. Integrated
711 analysis of multimodal single-cell data. *Cell.* 2021;184(13):3573-87 e29.
712 37. Choudhary S, and Satija R. Comparison and evaluation of statistical error models for
713 scRNA-seq. *Genome Biol.* 2022;23(1):27.
714 38. Cheng C, Easton J, Rosencrance C, Li Y, Ju B, Williams J, et al. Latent cellular analysis
715 robustly reveals subtle diversity in large-scale single-cell RNA-seq data. *Nucleic Acids Res.*
716 2019;47(22):e143.
717 39. Finak G, McDavid A, Yajima M, Deng J, Gersuk V, Shalek AK, et al. MAST: a flexible
718 statistical framework for assessing transcriptional changes and characterizing heterogeneity
719 in single-cell RNA sequencing data. *Genome Biol.* 2015;16:278.
720 40. Fumarola C, La Monica S, Alfieri RR, Borra E, and Guidotti GG. Cell size reduction
721 induced by inhibition of the mTOR/S6K-signaling pathway protects Jurkat cells from
722 apoptosis. *Cell Death Differ.* 2005;12(10):1344-57.
723 41. La Monica S, Galetti M, Alfieri RR, Cavazzoni A, Ardizzoni A, Tiseo M, et al. Everolimus
724 restores gefitinib sensitivity in resistant non-small cell lung cancer cell lines. *Biochem*
725 *Pharmacol.* 2009;78(5):460-8.
726 42. Gennady Korotkevich VS, Nikolay Budin, Boris Shpak, Maxim N. Artyomov, Alexey
727 Sergushichev. Fast gene set enrichment analysis. *bioRxiv.* 2021.
728 43. Vasaikar SV, Deshmukh AP, den Hollander P, Addanki S, Kuburich NA, Kudaravalli S, et
729 al. EMTome: a resource for pan-cancer analysis of epithelial-mesenchymal transition genes
730 and signatures. *Br J Cancer.* 2021;124(1):259-69.

731 44. Cavazzoni A, Alfieri RR, Carmi C, Zuliani V, Galetti M, Fumarola C, et al. Dual
732 mechanisms of action of the 5-benzylidene-hydantoin UPR1024 on lung cancer cell lines.
733 *Mol Cancer Ther.* 2008;7(2):361-70.

734

735 **Figure Legends**

736 **Figure 1. A) Immunophenotypic characterization of tumor tissues, cell lines and PDX of**
737 **CUP#55.** Hematoxylin-eosin (HE), keratin7 (K7) and keratin20 (K20) IHC staining was reported for
738 tumor tissue, cell lines and PDX in CUP#55 model (40x). The staining showed that cell line and PDX
739 models recapitulated the histology of the tumor tissue. **B) Immunophenotypic characterization of**
740 **tumor tissues, cell lines and PDX of CUP#96.** Hematoxylin-eosin (HE), keratin7 (K7) and keratin20
741 (K20) IHC staining was reported for tumor tissue, cell lines and PDX in CUP#96 model (40x).
742 CUP#96 cell line grows forming tumoroid structures. The staining showed that cell line and PDX
743 models recapitulated the histology of the tumor tissue.

744 **Figure 2. CUP models characterization.** A) Immunophenotypic analysis of CUP #55 and #96 cell
745 lines demonstrating the expression of cancer stem cell markers CD44 and EPCAM. Staining: nucleus
746 (DAPI, blue), CD44 and EPCAM (green). B) Gene expression analysis of stemness genes in CUP#55
747 and CUP#96. Bars represent the ratio between the gene copies and the reference HPRT copies
748 assessed by ddPCR. The expression in CUP cell lines was compared to other cancer cell lines from
749 lung and melanoma origin.

750 **Figure 3. Single cell transcriptome analysis of CUP#55. A)** Cell clustering based on the similarity
751 among expression profiles, obtained through the scLCA method; cells are separated in two distinct
752 clusters **B)** Scores computed by the scType method for putative tissues of origin for CUP#55 cells
753 **C)** MetaCore pathway analysis of genes markers of T/NK cells. Differentially expressed genes were
754 imported into MetaCore analytical software to determine the significantly enriched pathways in T/NK
755 cells, which are mostly related to cell division and DNA repair.

756 **Figure 4. Single cell gene expression.** The panels show the expression and distribution in CUP#55
757 single cells of the FGFR2 gene and other selected markers expressed in liver cancer stem cells and
758 involved in the EMT process.

759 **Figure 5. FGFR2 amplification in CUP models.** A) FISH analysis shows the different nature of
760 FGFR2 amplification in the two CUP cell models: double minutes for CUP#96 and HSR for CUP#55;
761 FGFR2 gene probe is in red, Chr10 centromere probe in green, nucleus in blue. B) Copy number
762 variation (CNV) analysis of FGFR2 gene detected by ddPCR using a probe-based assay. C) FGFR2
763 gene expression in the two amplified models and a control not amplified cell line. Bars represent the
764 ratio between the gene copies and the reference HPRT copies assessed by ddPCR. D) Evaluation by
765 western blot analysis of total and phosphorylated forms of FGFR2 in CUP#55 and #96, compared to
766 the H1581 NSCLC cell line.

767 **Figure 6. *In vitro* FGFR2 targeting and synergic activity of FGFR2 and MEK inhibitors in**
768 **CUP#55.** A) CUP#55 cells were treated with BGJ398 at the indicated concentrations; after 24h,
769 protein extracts were analyzed by Western blotting for the indicated proteins. The results are
770 representative of two independent experiments; B) CUP#55 cells were incubated with BGJ398 1μM,
771 trametinib 100 nM, or the combination; after 24h, protein extracts were analyzed by Western blotting
772 for the indicated proteins. The results are representative of two independent experiments; C) CUP#55
773 cells were treated with increasing concentrations of BGJ398 in combination with trametinib 100 nM.
774 After 96h, cell proliferation was assessed by MTS assay. The data are expressed as percent inhibition
775 vs. control. The asterisks indicate the statistical significance vs. the corresponding points of the Bliss
776 Theoretical curve. The results are representative of three independent experiments; D) CUP#55 cells
777 were incubated with BGJ398 1μM and/or trametinib 100 nM; after 96h, the percentage of cell death
778 was evaluated by fluorescence microscopy after Hoechst 33342/PI staining. The data are mean values
779 ±SD of three independent experiments. **$p<0.01$, ***$p<0.001$.

780 **Figure 7. *In vitro* FGFR2 targeting and synergic activity of FGFR2 and MEK inhibitors in**
781 **CUP#96.** A) CUP#96 cells were treated with BGJ398 at the indicated concentrations; after 24h,
782 protein extracts were analyzed by Western blotting for the indicated proteins. The results are
783 representative of two independent experiments; B) CUP#96 cells were incubated with BGJ398 100

784 nM, trametinib 10 nM or the combination; after 24h, protein extracts were analyzed by Western
785 blotting for the indicated proteins. The results are representative of two independent experiments; C)
786 CUP#96 cells were treated with increasing concentrations of BGJ398 in combination with trametinib
787 10 nM. After 96h, cell proliferation was assessed by MTS assay. The data are expressed as percent
788 inhibition vs. control. The asterisks indicate the statistical significance vs. the corresponding points
789 of the Bliss Theoretical curve. The results are representative of three independent experiments; D)
790 CUP#96 cells were incubated with BGJ398 100 nM and/or trametinib 10 nM; after 96h, the
791 percentage of cell death was evaluated by fluorescence microscopy after Hoechst 33342/PI staining.
792 The data are mean values ±SD of three independent experiments. *$p<0.05$; **$p<0.01$, ***$p<0.001$,
793 ****$p < 0.0001$.

794 **Figure 8. *In vivo* activity of FGFR2 and MEK inhibitors.** *In vivo* treatment of A) PDX#96 PDXs
795 and B) PDX#55 PDXs. The timeline shows the day of tumor volume measurement, and the color bars
796 represent the scheme of each treatment. The line graph shows that the combination of
797 trametinib+BGJ398 treatments (purple) is more effective than the single ones (trametinib in red and
798 BGJ398 in blue) in both PDX models. N=5 mice per group. *$p<0.05$, **$p<0.01$, ***$p<0.001$,
799 ****$p<0.0001$.

800

801

802

803 **Tables with titles and legends**

804

805 **Table 1. Genetic alterations detected in CUP#55 patient-derived tissues and models**

806

Gene	coding change	aminoacidic change	tumor FFPE	ccfDNA at diagnosis	ccfDNA at disease progression	cell line	PDX Passage1	predicted as pathogenic*
ALK	c.A1301G	p.K434R	not detected	not detected	7.0%	not detected	not detected	no
APC	4607insA	p.T1556fs*3	9.8%	22.6%	29.9%	100.0%	95.0%	ND
APC	c.A2659C	p.S887R	not detected	not detected	not detected	43.2%	not detected	yes
ARID1A	c.C3826T	p.R1276X	8.9%	28.5%	22.8%	53.0%	19.8%	yes
CREBBP	c.T1448C	p.L483P	not detected	not detected	not detected	not detected	21.7%	ND
DOT1L	c.A1193C	p.K398T	not detected	not detected	not detected	38.2%	not detected	yes
EP300	c.A7118C	p.N2373T	not detected	not detected	not detected	not detected	32.2%	no
EPHA5	c.A1417C	p.T473P	not detected	not detected	8.3%	not detected	not detected	no
ERBB3	c.C384A	p.S128R	9.8%	20.7%	20.4%	41.09%	48.60%	yes
ERBB4	c.T343A	p.Y115N	not detected	not detected	not detected	not detected	33.8%	yes
FAT1	c.A2084C	p.N695T	not detected	not detected	2.6%	not detected	not detected	no

GRIN2A	c.A4064C	p.K1355T	not detected	not detected	not detected	not detected	22.3%	no
KDM5A	c.T3547C	p.W1183R	not detected	not detected	not detected	not detected	22.2%	yes
KDR	c.A981C	p.K327N	not detected	not detected	not detected	not detected	27.9%	ND
KEAP1	c.G404A	p.R135H	9.0%	22.6%	19.5%	51.8%	44.0%	yes
KMT2C	c.C2459T	p.T820I	not detected	1.1%	1.1%	not detected	not detected	yes
KMT2C	c.C1013T	p.S338L	not detected	5.5%	4.3%	not detected	not detected	no
KMT2C	c.C2689T	p.R897X	not detected	not detected	1.4%	not detected	not detected	yes
KMT2C	c.C2228T	p.P743L	not detected	not detected	1.6%	not detected	not detected	no
MED12	c.A688C	p.I230L	not detected	not detected	not detected	not detected	25.0%	no
MGA	c.A395C	p.N132T	not detected	not detected	not detected	not detected	30.5%	yes
MGA	c.T4004C	p.L1335P	not detected	not detected	1.6%	not detected	not detected	ND
NF1	c.A6083G	p.K2028R	not detected	not detected	not detected	not detected	25.4%	yes
NTRK1	c.C2206T	p.Q736X	8.3%	26.0%	22.3%	32.6%	44.7%	yes
PALB2	C2419T	p.P807S	9.0%	19.1%	16.6%	not detected	47.4%	no
PTPRD	c.T2908G	p.L970V	not detected	5.1%	3.5%	not detected	47.7%	yes
PTPRD	c.A3117C	p.Q1039H	not detected	not detected	6.8%	not detected	not detected	yes
PTPRT	c.T479C	p.F160S	not detected	not detected	not detected	not detected	33.8%	no
RBM10	c.A2024G	p.K675R	not detected	not detected	not detected	not detected	41.7%	no

TP53	c.C9G	p.C3W	not detected	1.2%	not detected	not detected	not detected	yes
TP53	c.A355G	p.I119V	not detected	1.7%	not detected	not detected	not detected	yes
TP53	c.G315C	p.M105I	not detected	1.8%	not detected	not detected	not detected	yes
TP53	c.T316C	p.C106R	not detected	2.1%	not detected	not detected	not detected	yes
ZFHX3	c.A1604C	p.E535A	not detected	not detected	not detected	not detected	27.5%	no
ZFHX3	c.A7529G	p.Q2510R	not detected	not detected	not detected	not detected	39.7%	no

807 *variants were considered pathogenic when more than 50% of the 8 predictors (SIFT, Polyphen2 HVAR, LRT, Mutation Taster, Mutation Assessor, FATHMM,
808 CADD and VEST) considered the alteration as pathogenic/damaging/deleterious/harmful. ND= not defined

809

810

811 **Table 2. Genetic alterations detected in CUP#96 patient-derived tissues and models**

812

Gene	coding change	aminoacidic change	CUP#96 cell line	ccfDNA at diagnosis	predicted as pathogenic *
PIK3C2G	c.G1813A	p.V605I	100.00%	48.35%	no
TP53	c.G418A	p.V140M	100.00%	49.34%	yes
SMAD4	c.A1610G	p.D537G	100.00%	44.23%	yes
KMT2C	c.G943A	p.G315S	4.58%	5.31%	yes

CTNNB1	c.C110T	p.S37F	55.10%	22.39%	yes
KMT2C	c.A2725G	p.R909G	-	6.48%	yes
KMT2C	c.C3274T	p.R1092X	-	5.28%	yes
KMT2C	c.C1013T	p.S338L	-	4.57%	no
KMT2C	c.G944A	p.G315D	-	3.09%	yes

813 *variants were considered pathogenic when more than 50% of the 8 predictors (SIFT, Polyphen2 HVAR, LRT, Mutation Taster, Mutation Assessor, FATHMM,

814 CADD and VEST) considered the alteration as pathogenic/damaging/deleterious/harmful. ND= not defined

815

816

817

818

Figure 1

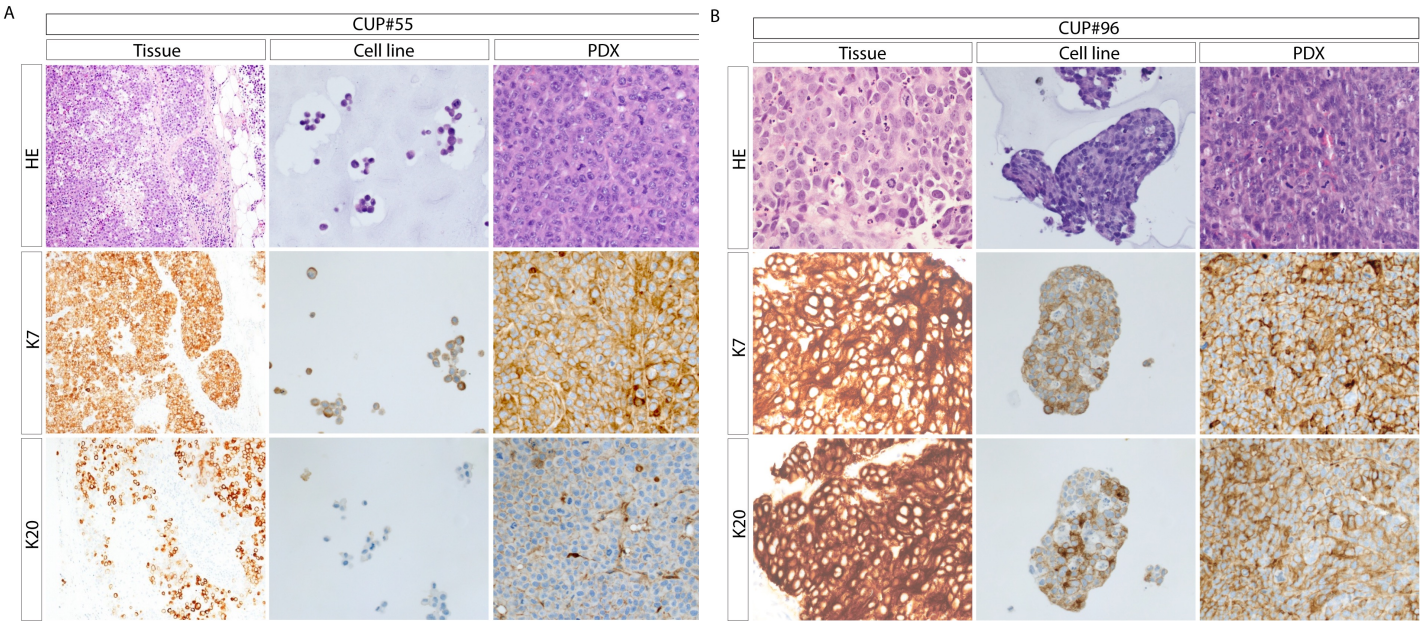
A
CUP#55
Tissue
Cell line
PDX
HE
K7
K20
B
CUP#96
Tissue
Cell line
PDX
HE
K7
K20

Figure 2

A

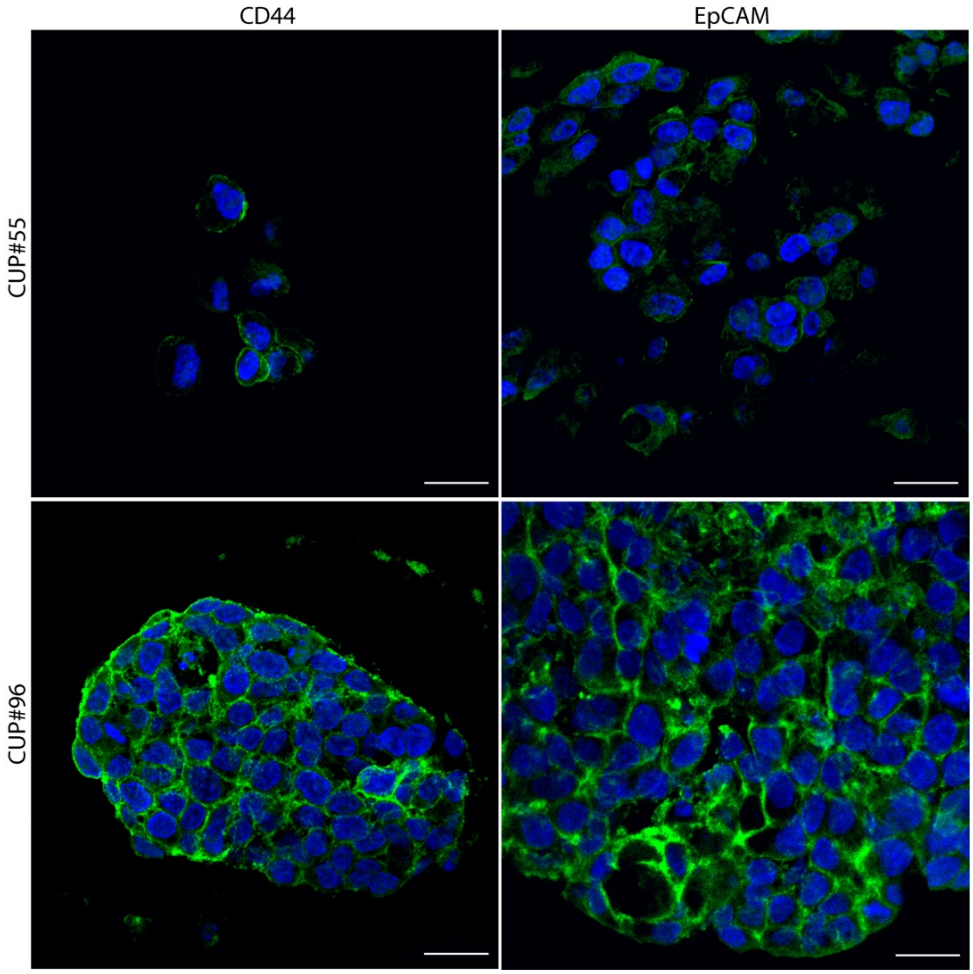
CD44
EpCAM
CUP#55
CUP#96

B

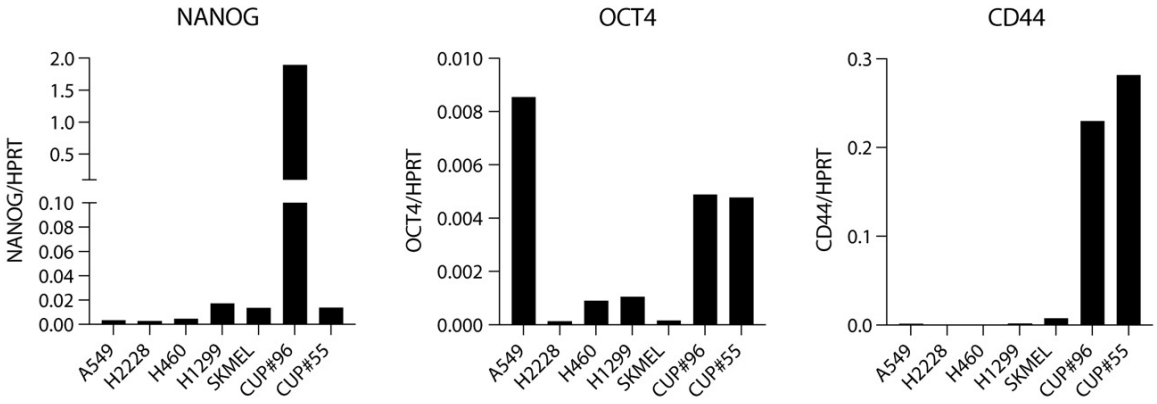
NANOG
OCT4
CD44
NANOG/HPRT
OCT4/HPRT
CD44/HPRT
2.0
1.5
1.0
0.5
0.10
0.08
0.06
0.04
0.02
0.00
0.010
0.008
0.006
0.004
0.002
0.000
0.3
0.2
0.1
0.0
A549
H2228
H460
H1299
SKMEL
CUP#96
CUP#55

Figure 3

A

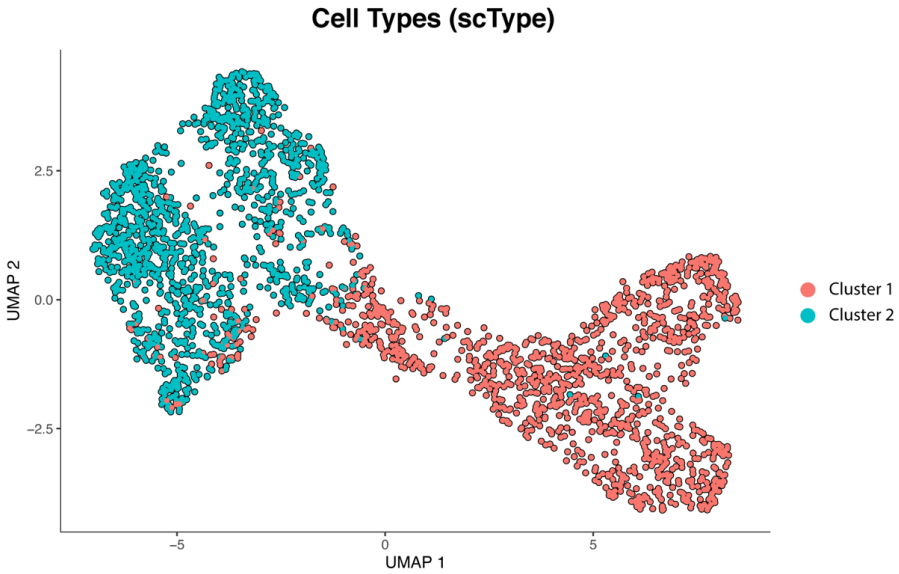
Cell Types (scType)
UMAP 2
2.5
0.0
−2.5
−5
0
5
UMAP 1
Cluster 1
Cluster 2

B

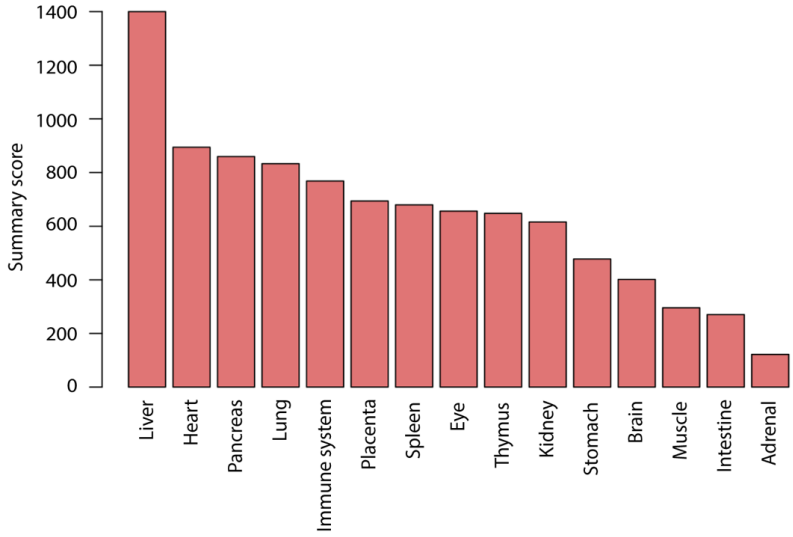
Summary score
1400
1200
1000
800
600
400
200
0
Liver
Heart
Pancreas
Lung
Immune system
Placenta
Spleen
Eye
Thymus
Kidney
Stomach
Brain
Muscle
Intestine
Adrenal

C

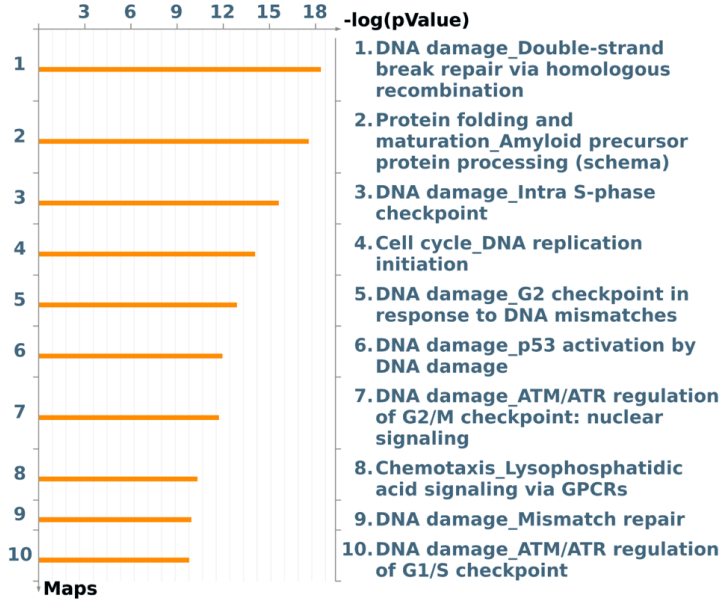
3
6
9
12
15
18
-log(pValue)
1
2
3
4
5
6
7
8
9
10
Maps
1. DNA damage_Double-strand break repair via homologous recombination
2. Protein folding and maturation_Amyloid precursor protein processing (schema)
3. DNA damage_Intra S-phase checkpoint
4. Cell cycle_DNA replication initiation
5. DNA damage_G2 checkpoint in response to DNA mismatches
6. DNA damage_p53 activation by DNA damage
7. DNA damage_ATM/ATR regulation of G2/M checkpoint: nuclear signaling
8. Chemotaxis_Lysophosphatidic acid signaling via GPCRs
9. DNA damage_Mismatch repair
10. DNA damage_ATM/ATR regulation of G1/S checkpoint

Figure 4

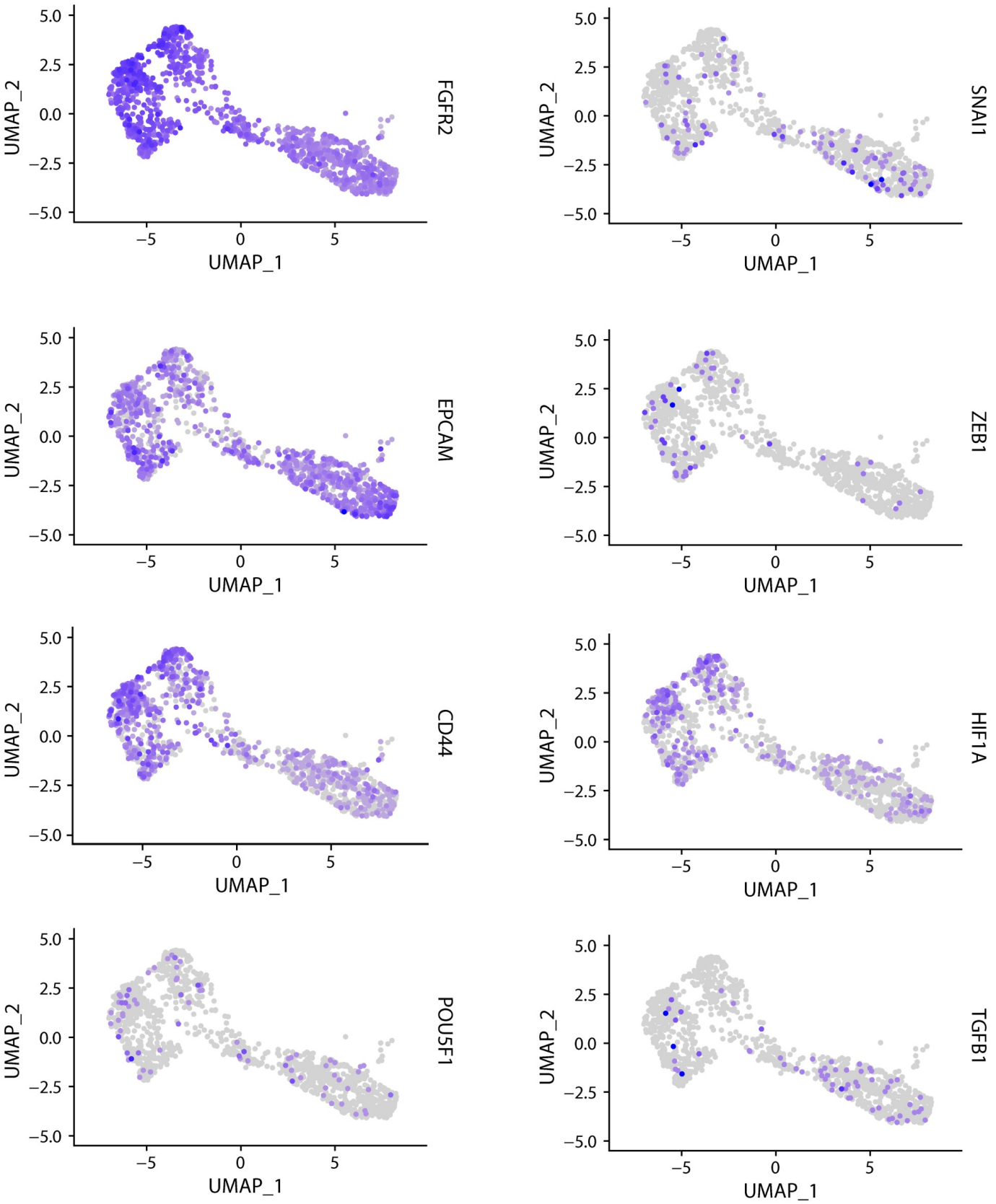
FGFR2
SNAI1
EPCAM
ZEB1
CD44
HIF1A
POU5F1
TGFB1
UMAP_1
UMAP_2
5.0
2.5
0.0
−2.5
−5.0
−5
0
5

Figure 5

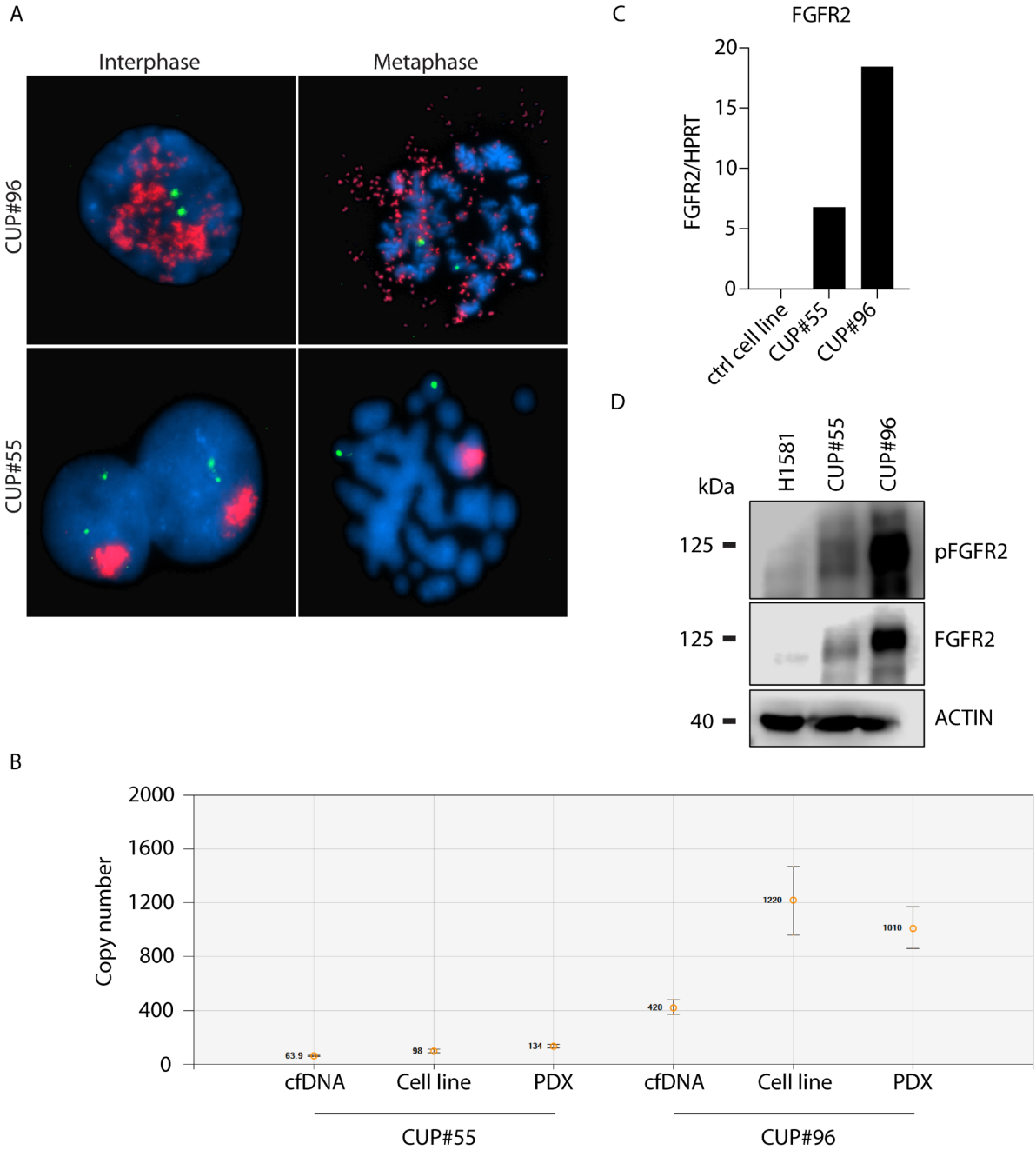
A
Interphase
Metaphase
CUP#96
CUP#55
C
FGFR2
FGFR2/HPRT
20
15
10
5
0
ctrl cell line
CUP#55
CUP#96
D
kDa
H1581
CUP#55
CUP#96
125
pFGFR2
125
FGFR2
40
ACTIN
B
Copy number
2000
1600
1200
800
400
0
63.9
98
134
420
1220
1010
cfDNA
Cell line
PDX
cfDNA
Cell line
PDX
CUP#55
CUP#96

Figure 6

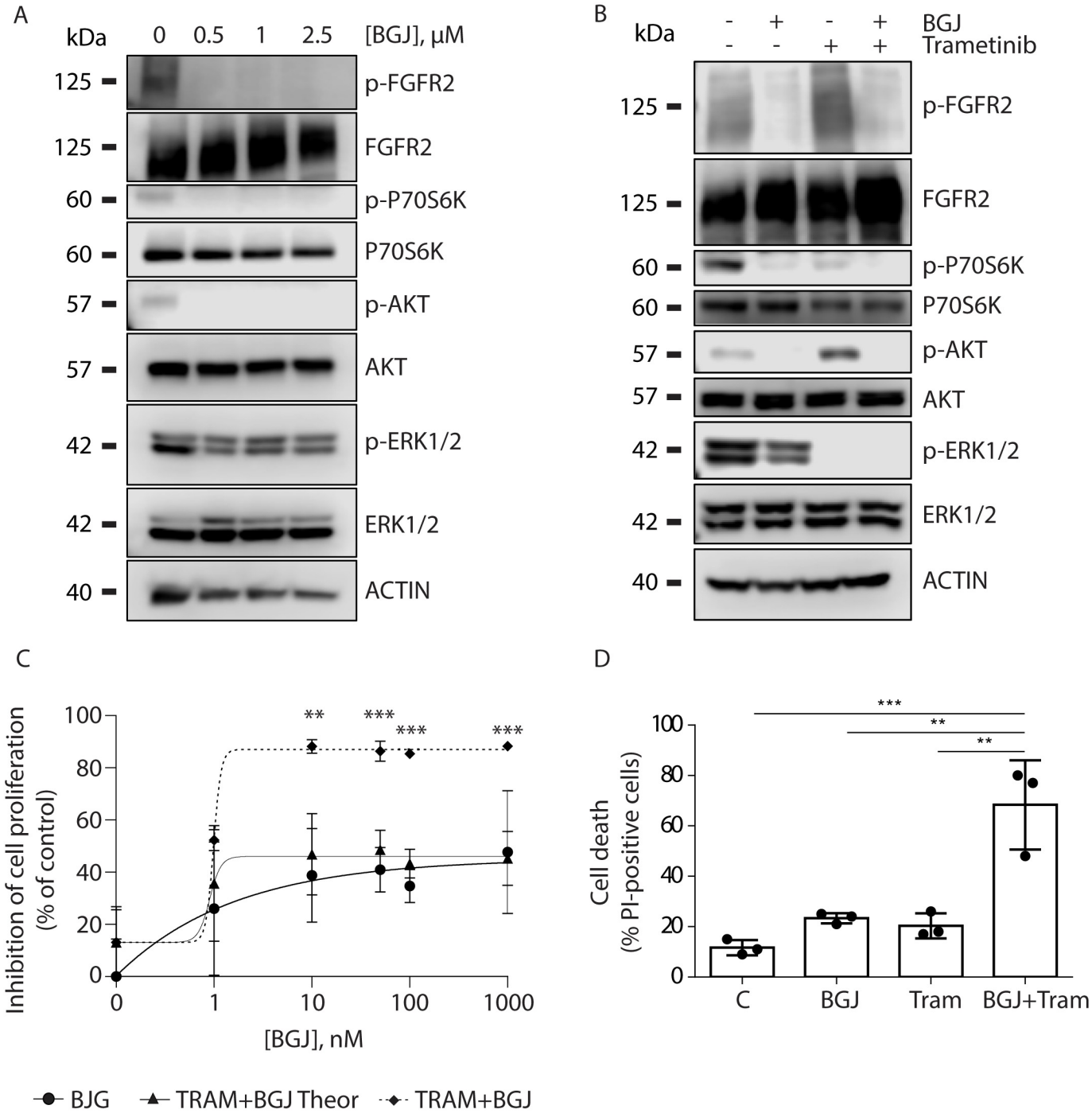
A
kDa
0
0.5
1
2.5
[BGJ], μM
125
p-FGFR2
125
FGFR2
60
p-P70S6K
60
P70S6K
57
p-AKT
57
AKT
42
p-ERK1/2
42
ERK1/2
40
ACTIN
B
kDa
BGJ
Trametinib
125
p-FGFR2
125
FGFR2
60
p-P70S6K
60
P70S6K
57
p-AKT
57
AKT
42
p-ERK1/2
42
ERK1/2
40
ACTIN
C
Inhibition of cell proliferation (% of control)
[BGJ], nM
BJG
TRAM+BGJ Theor
TRAM+BGJ
D
Cell death (% PI-positive cells)
C
BGJ
Tram
BGJ+Tram

Figure 7

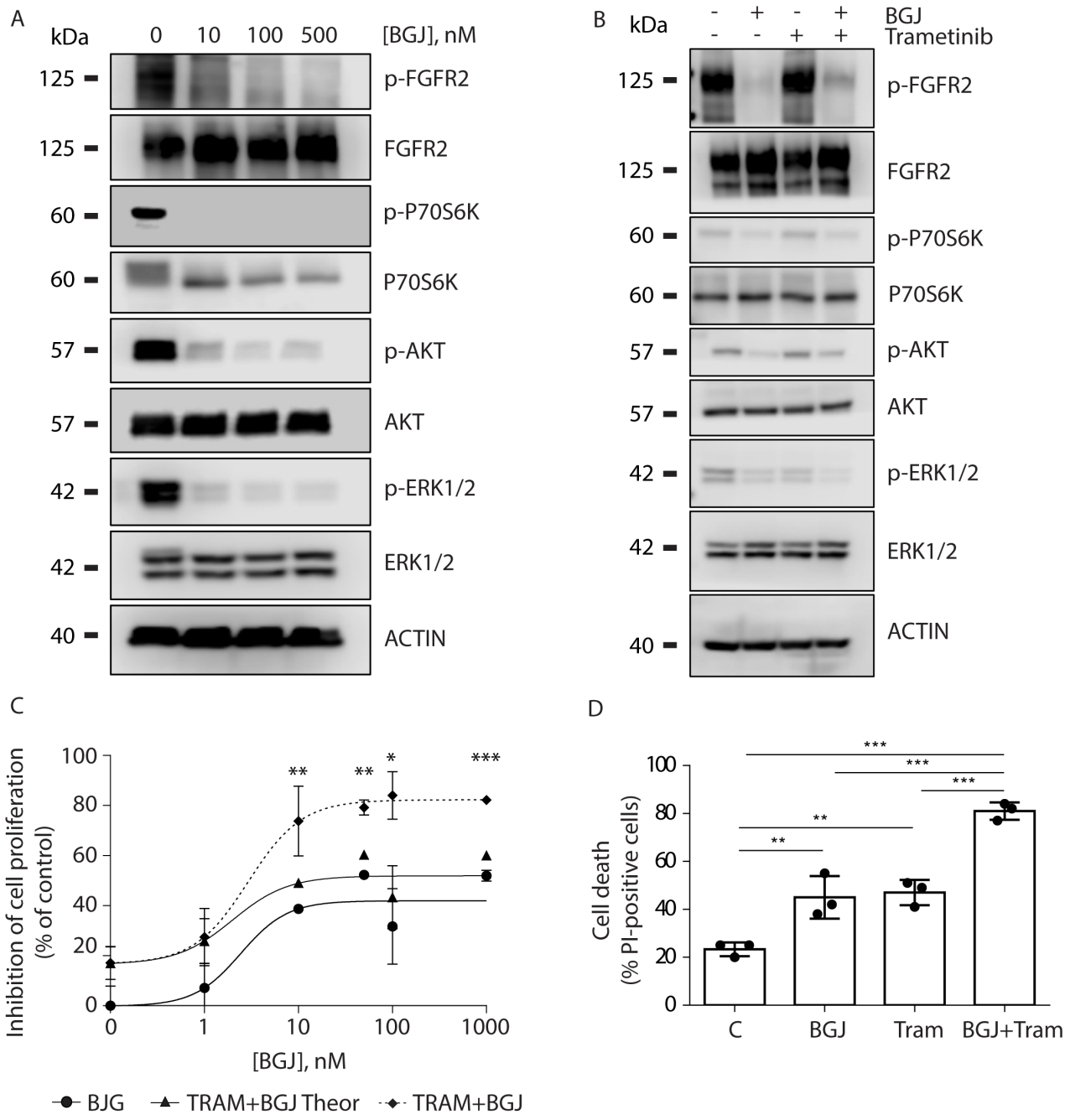
A
kDa
0
10
100
500
[BGJ], nM
125
p-FGFR2
125
FGFR2
60
p-P70S6K
60
P70S6K
57
p-AKT
57
AKT
42
p-ERK1/2
42
ERK1/2
40
ACTIN
B
kDa
BGJ
Trametinib
125
p-FGFR2
125
FGFR2
60
p-P70S6K
60
P70S6K
57
p-AKT
57
AKT
42
p-ERK1/2
42
ERK1/2
40
ACTIN
C
Inhibition of cell proliferation
(% of control)
[BGJ], nM
BJG
TRAM+BGJ Theor
TRAM+BGJ
D
Cell death
(% PI-positive cells)
C
BGJ
Tram
BGJ+Tram

Figure 8

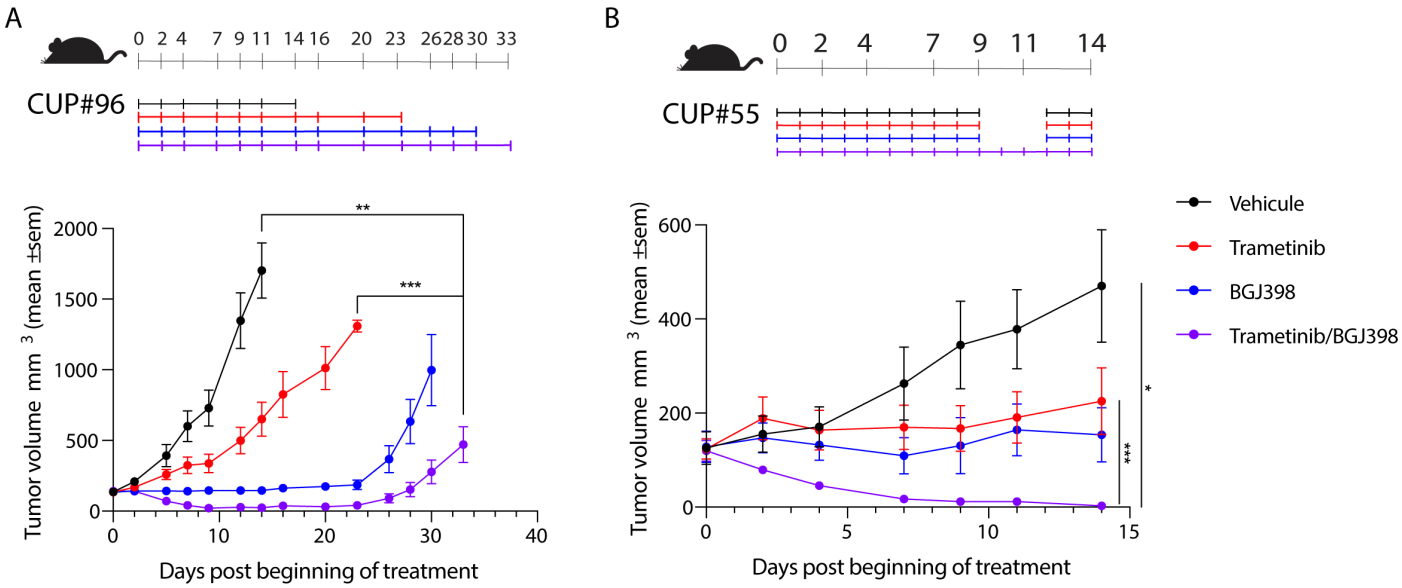
A
0 2 4 7 9 11 14 16 20 23 26 28 30 33
CUP#96
Tumor volume mm 3 (mean ±sem)
2000
1500
1000
500
0
**
***
0
10
20
30
40
Days post beginning of treatment
B
0 2 4 7 9 11 14
CUP#55
Tumor volume mm 3 (mean ±sem)
600
400
200
0
***
*
0
5
10
15
Days post beginning of treatment
Vehicule
Trametinib
BGJ398
Trametinib/BGJ398

Supplemental Figures titles and legends

Figure S1. Brightfield representative images of cultured cell lines growing as in suspension 3D-structures. CUP cell lines display discrete *in vitro* growth characteristics. CUP#96 grow as tightly compact spheroids and require trypsinization for passaging. CUP#55 forms loosely aggregated and weakly tight strands requiring only gentle mechanical dissociation for disaggregation. All established cell lines remain viable after freezing and thawing at various passages (self-renew more than 20 passages). Scalebar: 9000um.

Figure S2. CUP#96 cell growth. A) Panel of brightfield images acquired every 24h for 10 days, in blue the mask used for the object area measurements. B) Growth curve obtained for CUP#96 spheroid analyzing images acquired every 6 hours.

Figure S3. CUP#55 cell growth. A) Panel of brightfield images acquired every 24h for 10 days, in blue the mask used for the object area measurements. B) Growth curve obtained for CUP#55 cluster analyzing images acquired every 6 hours.

Figure S4. Relative body weight (RBW) graph. Graph showing the RBW over time of N=5 mice for CUP#96 (upper panel) and CUP#55 (lower panel) PDX models. CUP#96 PDX showed a regular RBW for the entire duration of treatments instead CUP#55 PDX were sacrificed after 14 days due to cachexia induced by the tumor.

Figure S5. FigureS5 Single cell transcriptomic analysis of CUP#55. A) Cell type identification applying a reference-based classification based on a liver cell atlas (Azimuth software) showed two distinct subgroups: cholangiocytes and T/NK cells B) Cell cycle phase of single cells: cell cycle has a cofounding effect in the identification of the T/NK subgroup.

Figure S6. Functional classification of CUP#55 cluster markers. A) Pathway enrichment analysis of positive marker genes characterizing cluster1 and B) of cluster 2. Marker genes ($P < 0.05$) were imported into MetaCore analytical software to determine significantly enriched pathways in each group.

Figure S7. FGFR2 genomic alterations in AACR GENIE (A) and MSK-IMPACT (B) cancer types with frequency > 3%. Cancers of unknown primary were tested for genomic alterations in Zehir et al study *(16)* and AACR project GENIE *(17)*. In these studies, FGFR2 genomic alterations were detectable with a frequency of about 3-4%. The most frequent alterations were mutations, fusions, and amplifications.

Figure S8. FGFR2 isoforms detection in the two cell models and a control not amplified cell line. ddPCR was used to measure the abundance of two distinct isoforms of FGFR2: FGFR2IIIb epithelial and FGFR2IIIc mesenchymal. CUP#55 and CUP#96 showed higher level of FGFR2IIIb but both expressed also the mesenchymal one suggesting an epithelial-mesenchymal transition of the cells.

Figure S9. Viability assay of CUP#55 model exposed to different concentrations of FGFR2 inhibitors. Viability reduction of CUP#55 cell line after treatment with FGFR inhibitors (BGJ398, Ponatinib, Dovitinib) or cisplatin. Data were obtained using CellTiter-Glo Luminescent Cell Viability Assay (Promega).

Figure S10. Cell death assessment upon treatment with FGFR2 and MEK inhibitors. Representative images of CUP#55 cells untreated or treated with BGJ398 1μM and/or trametinib 100 nM for 96h and analyzed by fluorescence microscopy after Hoechst 33342/PI staining (Magnification 400X).

Figure S1

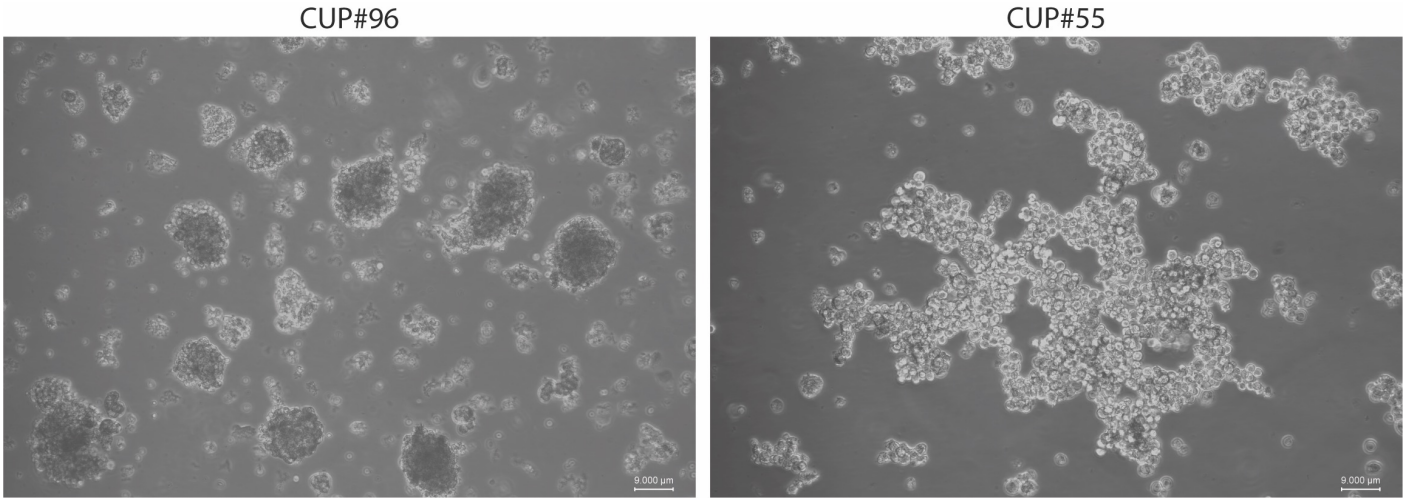

Figure S2

A CUP#96

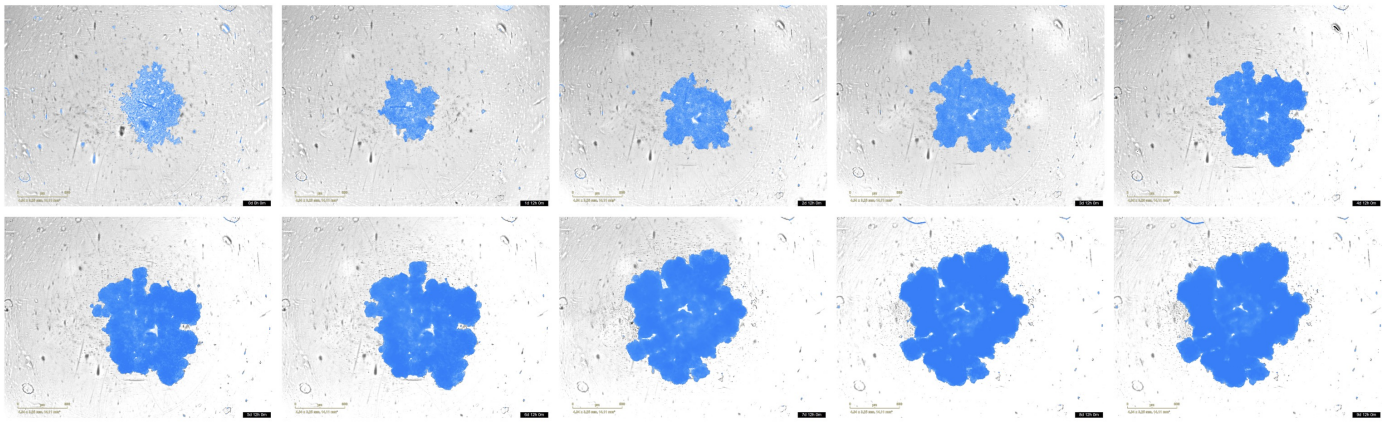

B

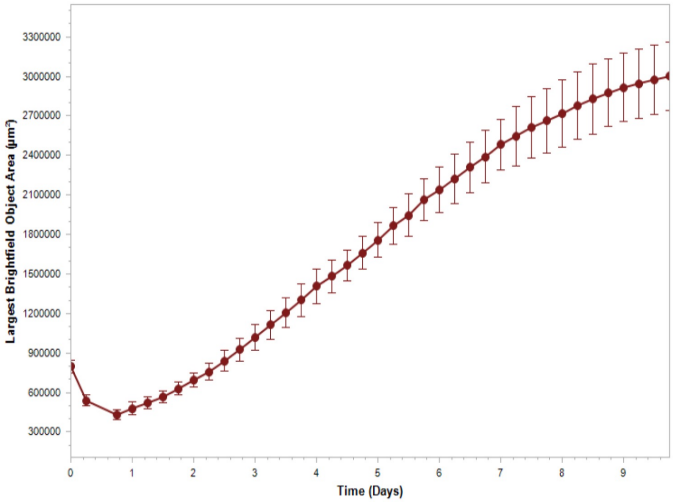

Figure S3

A CUP#55

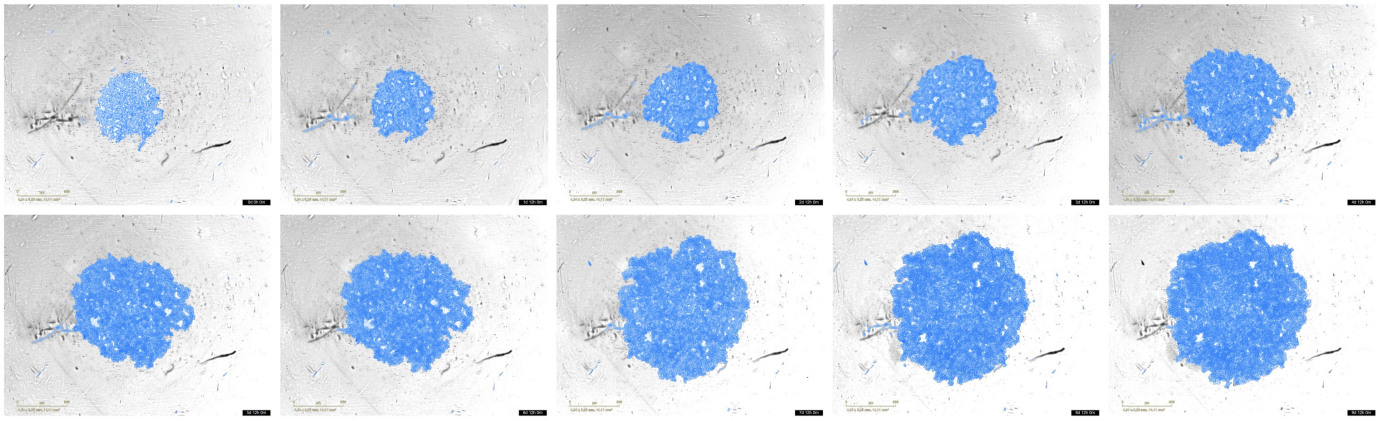

B

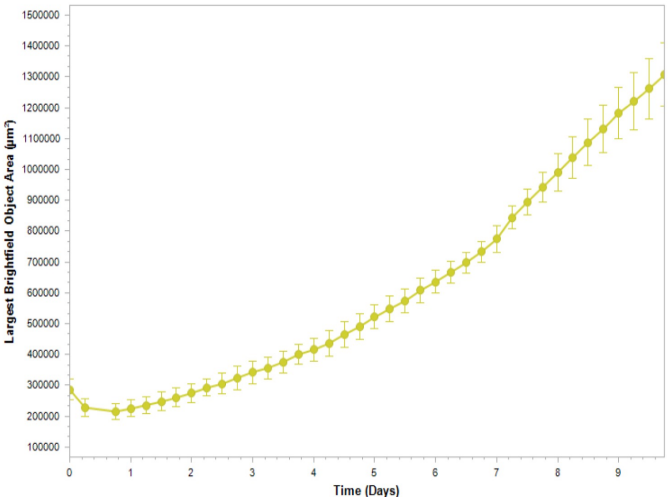

Figure S4

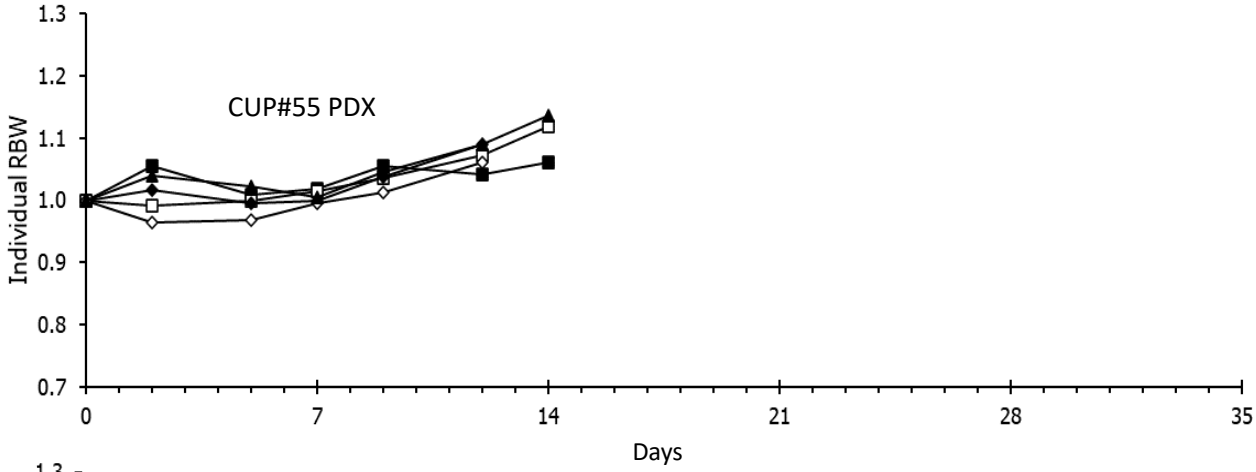

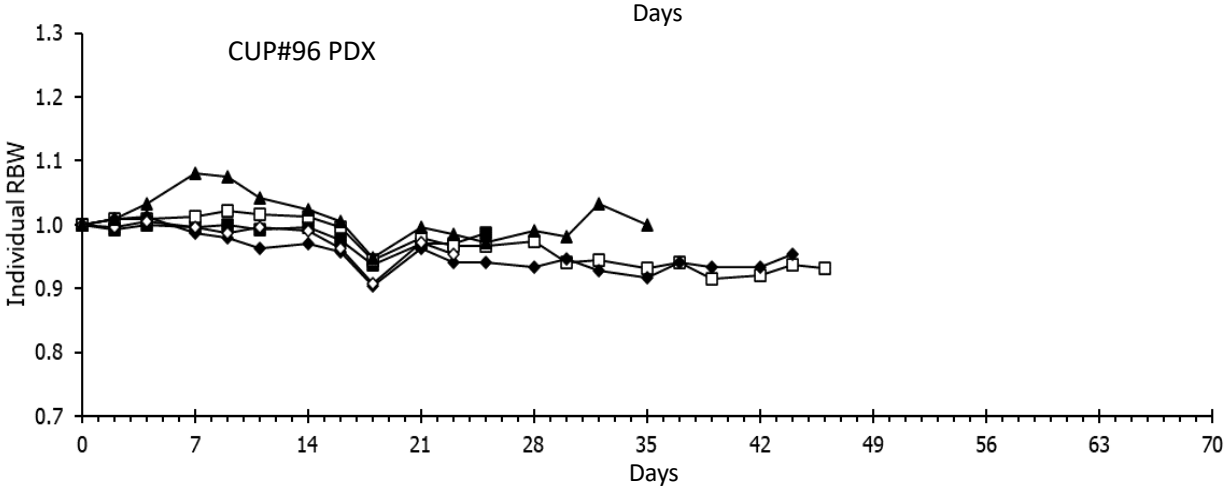

RBW= relative body weight

Figure S5

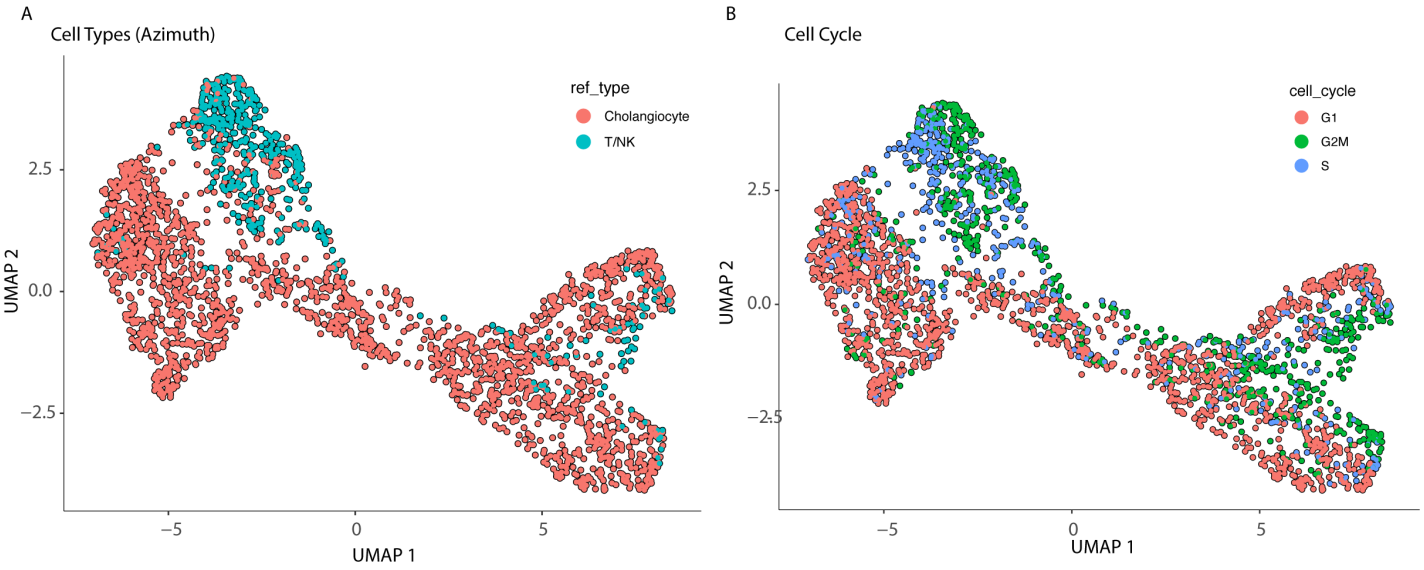
A
Cell Types (Azimuth)
ref_type
Cholangiocyte
T/NK
UMAP 2
UMAP 1
2.5
0.0
−2.5
−5
0
5
B
Cell Cycle
cell_cycle
G1
G2M
S
UMAP 2
UMAP 1
2.5
0.0
−2.5
−5
0
5

Figure S6

A

Cluster1

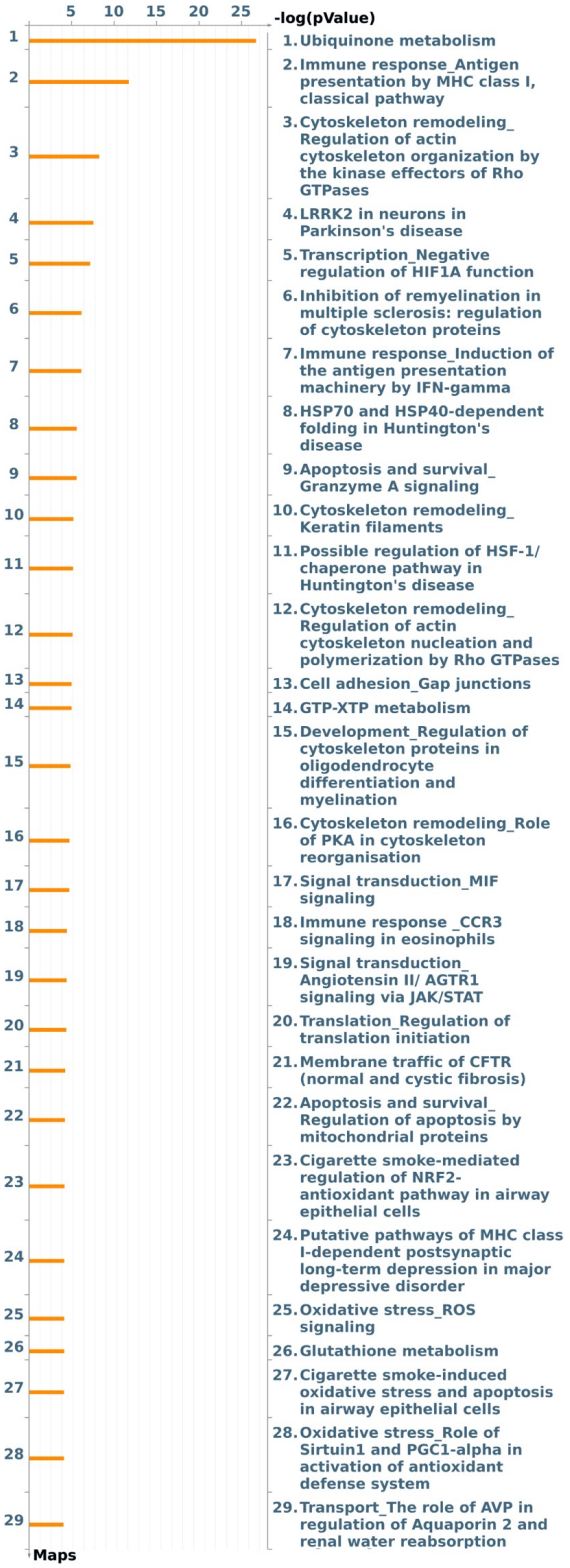

B

Cluster2

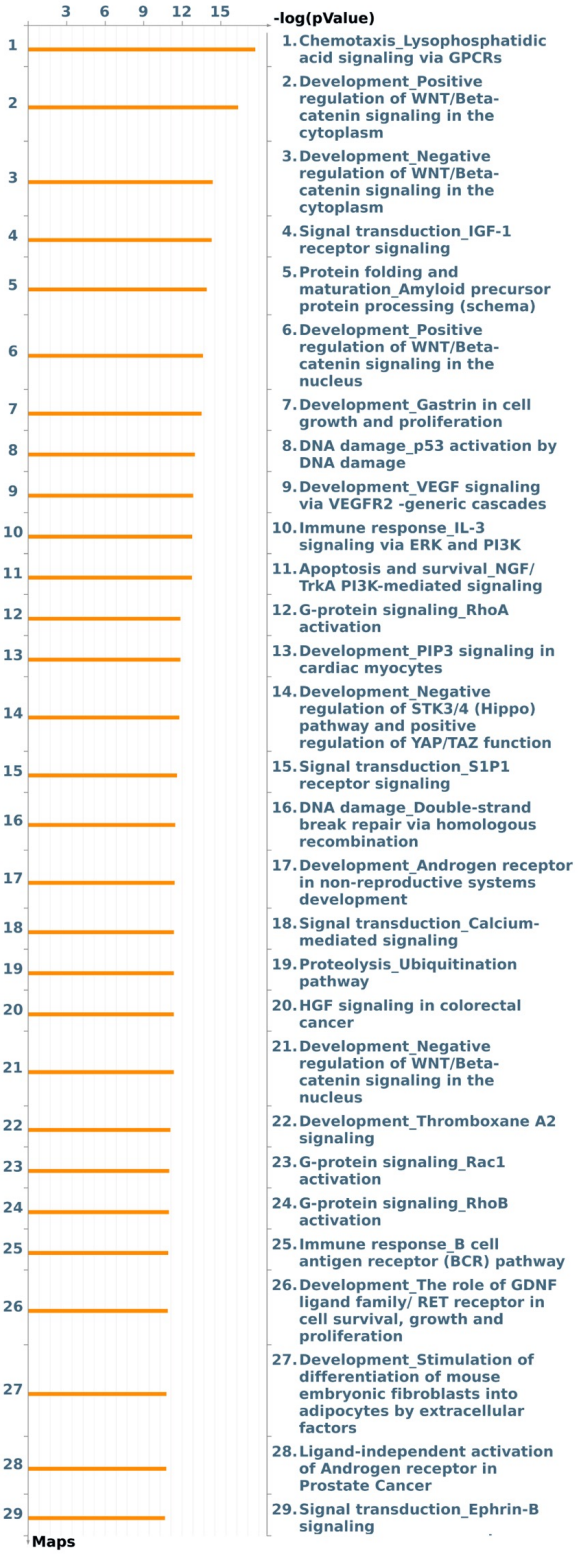

Figure S7

A

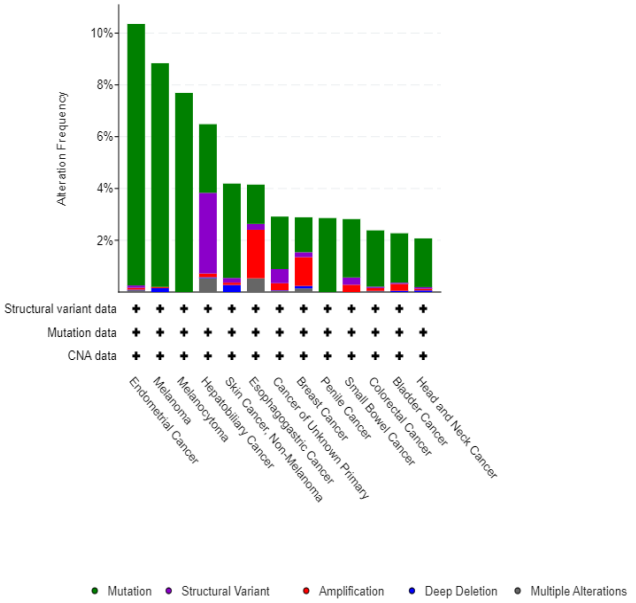
Alteration Frequency
10%
8%
6%
4%
2%
Structural variant data
Mutation data
CNA data
Endometrial Cancer
Melanoma
Melanocytoma
Hepatobiliary Cancer
Skin Cancer, Non-Melanoma
Esophagogastric Cancer
Cancer of Unknown Primary
Breast Cancer
Penile Cancer
Small Bowel Cancer
Colorectal Cancer
Bladder Cancer
Head and Neck Cancer
Mutation
Structural Variant
Amplification
Deep Deletion
Multiple Alterations

B

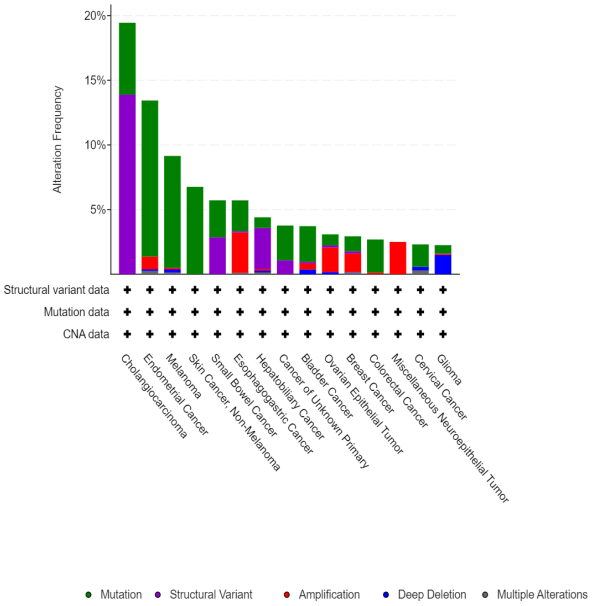
Alteration Frequency
20%
15%
10%
5%
Structural variant data
Mutation data
CNA data
Cholangiocarcinoma
Endometrial Cancer
Melanoma
Skin Cancer, Non-Melanoma
Small Bowel Cancer
Esophagogastric Cancer
Hepatobiliary Cancer
Cancer of Unknown Primary
Bladder Cancer
Ovarian Epithelial Tumor
Breast Cancer
Colorectal Cancer
Miscellaneous Neuroepithelial Tumor
Cervical Cancer
Glioma
Mutation
Structural Variant
Amplification
Deep Deletion
Multiple Alterations

Figure S8

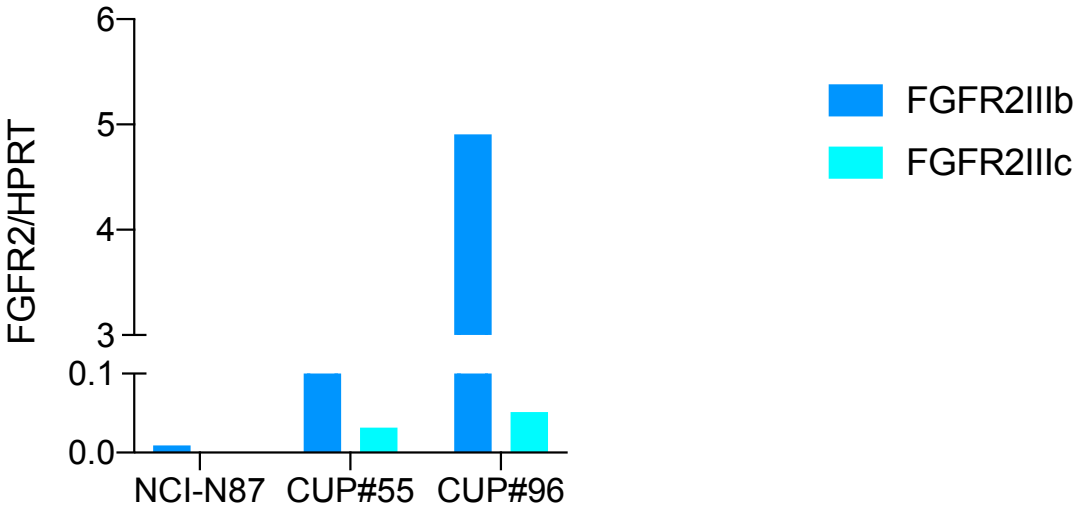
FGFR2/HPRT
6
5
4
3
0.1
0.0
NCI-N87
CUP#55
CUP#96
FGFR2IIIb
FGFR2IIIc

Figure S9

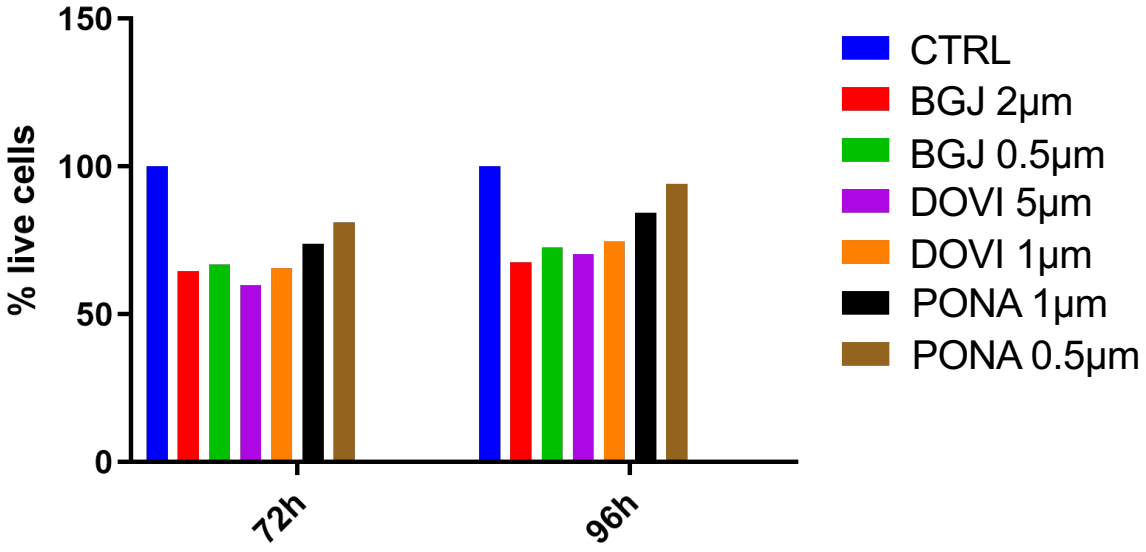
150
100
50
0
% live cells
72h
96h
CTRL
BGJ 2µm
BGJ 0.5µm
DOVI 5µm
DOVI 1µm
PONA 1µm
PONA 0.5µm

Figure S10

CUP#55

Control

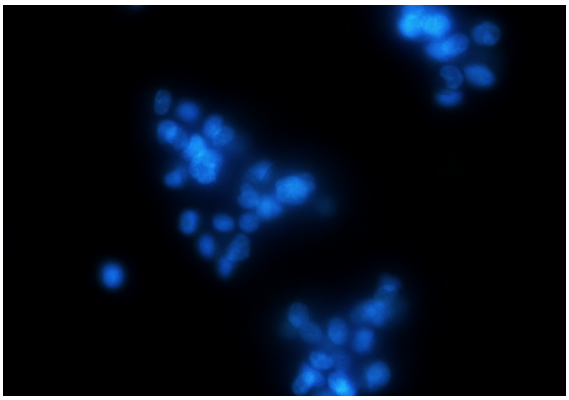

BGJ

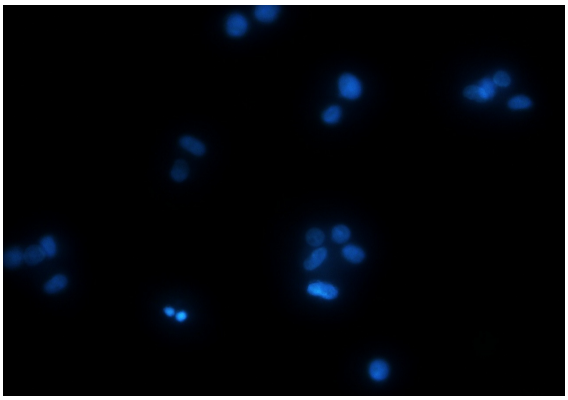

Tram

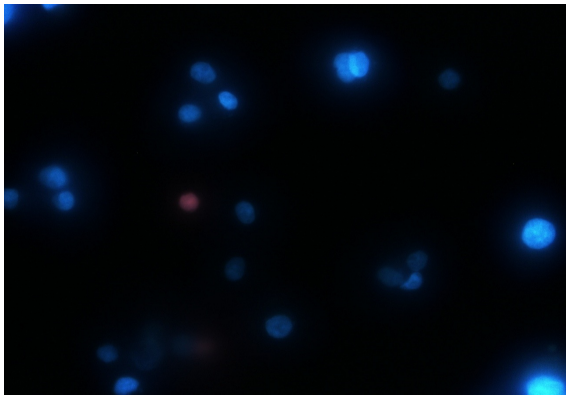

BGJ+Tram

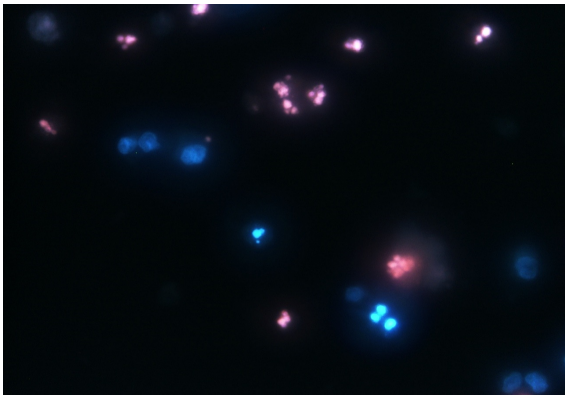

Table S1. CUP#55 Copy Number Variation analysis

chr	start	end	copy number	status	WilcoxonRankSumTest Pvalue	Cancer genes
1	155665260	249250621	3	gain	5.12765E-30	
2	103776840	105506454	8	gain	0.083802545	
2	102047226	103776840	3	gain	0.093389361	
4	0	19025754	1	loss	2.66313E-07	
4	162583716	164313330	5	gain	0.083802545	
5	84751086	108965682	1	loss	9.59798E-09	
5	74373402	83021472	4	gain	0.000116771	
6	38051508	46699578	3	gain	0.001639027	
7	91669542	159138663	3	gain	4.16267E-19	MET
7	65725332	89939928	3	gain	1.776E-06	
7	89939928	91669542	9	gain	0.083802545	
8	0	84751086	3	gain	3.39763E-22	
8	91669542	127991436	3	gain	8.74535E-15	MYC
8	127991436	146364022	4	gain	5.3776E-08	
8	84751086	91669542	5	gain	0.002754203	
9	0	5188842	3	gain	0.032354503	
10	121072980	122802594	4	gain	0.083802545	
10	122802594	124532208	38	gain	0.083802545	FGFR2
12	95128770	133851895	3	gain	1.40454E-12	
13	0	69184560	3	gain	1.42205E-17	
13	89939928	115169878	3	gain	1.29323E-09	
13	69184560	83021472	4	gain	2.43406E-06	
14	57077262	62266104	3	gain	0.006970193	
16	0	1729614	1	loss	0.08990996	
17	62266104	81195210	4	gain	6.34092E-08	
17	58806876	62266104	3	gain	0.016954397	
18	0	58806876	3	gain	3.04727E-17	
19	27673824	31133052	8	gain	0.014475979	CCNE1
X	108965682	155270560	3	gain	4.31504E-11	

Table S2. CUP#96 Copy Number Variation analysis

chr	start	end	copy number	status	WilcoxonRankSumTest Pvalue	Cancer genes
1	56274964	119826863	3	gain	7.47135E-29	
1	119826863	120311992	4	gain	0.084472944	
1	156696667	173676182	3	gain	4.06364E-13	
1	195506987	195992116	8	gain	0.083665749	
1	195992116	223159340	3	gain	3.45579E-11	
1	223159340	225584985	4	gain	0.003437108	
2	0	96055542	3	gain	1.64321E-37	ALK
2	109639154	110124283	5	gain	0.083665749	
2	132925346	133410475	5	gain	0.083665749	
2	171250537	238683468	3	gain	9.68663E-38	
3	42691352	53364190	1	loss	4.56062E-08	
3	195992116	198022430	1	loss	0.025631926	
4	38810320	41235965	1	loss	0.002621825	
4	41235965	41721094	15	gain	0.083665749	
4	162518215	163003344	8	gain	0.083665749	
5	91204252	91689381	8	gain	0.083665749	
5	101877090	102847348	3	gain	0.028275077	
5	112549928	114490444	0	loss	0.00053815	APC
5	172705924	173191053	3	gain	0.194703879	
5	173191053	173676182	8	gain	0.083665749	
5	173676182	180915260	1	loss	0.000553678	
6	21830805	24256450	3	gain	0.001732837	
6	37840062	85382704	3	gain	3.17326E-15	
6	90719123	91689381	4	gain	0.015348707	
6	91689381	132440217	3	gain	7.22454E-19	
6	132440217	132925346	4	gain	0.085286429	
7	0	11643096	3	gain	2.16274E-09	
7	11643096	12128225	9	gain	0.083665749	
7	12128225	13098483	5	gain	0.014432709	
7	13098483	90719123	3	gain	4.59954E-56	
7	90719123	91204252	15	gain	0.083665749	EGFR
7	91204252	159138663	3	gain	3.02665E-58	MET
8	47542642	94115026	3	gain	8.9215E-32	
8	94115026	94600155	7	gain	0.083665749	
8	94600155	105272993	3	gain	2.6545E-07	
8	105272993	121282250	4	gain	2.44038E-22	
8	121282250	132440217	5	gain	1.88069E-16	MYC
8	132440217	132925346	7	gain	0.083665749	
8	132925346	146364022	4	gain	3.96758E-17	
9	21345676	25711837	0	loss	2.13081E-07	CDKN2A, CDKN2B
9	71313963	136321249	3	gain	1.17325E-47	
9	136321249	136806378	6	gain	0.083665749	
9	136806378	138261765	3	gain	0.004438623	
10	49483158	49968287	4	gain	0.084472944	

10	122252508	122737637	83	gain	0.083464929	
10	122737637	123707895	714	gain	0.014369164	FGFR2
11	26682095	29107740	4	gain	0.000217254	
12	61126254	61611383	4	gain	0.084068562	
13	24256450	34444159	3	gain	1.36044E-11	
13	34444159	35414417	4	gain	0.014917243	
13	35414417	49968287	3	gain	1.19244E-11	
13	50938545	54334448	4	gain	0.000518798	
13	55789835	57245222	3	gain	0.003933076	
13	58700609	63066770	3	gain	9.07212E-05	
13	63066770	64037028	4	gain	0.016315498	
13	64037028	69373447	3	gain	4.93292E-05	
13	69373447	71313963	4	gain	0.000882443	
13	73739608	110609412	3	gain	4.08344E-29	
13	110609412	111094541	5	gain	0.083665749	
13	111094541	115169878	3	gain	0.00547465	
14	0	72769350	3	gain	1.88734E-46	
14	72769350	73254479	6	gain	0.083665749	
14	75680124	80531414	4	gain	1.69462E-07	
14	80531414	107349540	3	gain	4.0038E-25	
15	29107740	40265707	3	gain	3.13097E-07	
15	57245222	61611383	1	loss	3.84763E-07	
15	69858576	70828834	3	gain	0.020090686	
15	78105769	102531392	3	gain	5.51544E-13	
16	77135511	90354753	3	gain	1.82211E-08	
17	0	31048256	1	loss	5.90108E-11	
17	67432931	70828834	3	gain	7.94057E-05	
18	0	1940516	1	loss	0.069724351	
18	1940516	2425645	3	gain	0.100807894	
19	0	15038999	1	loss	4.58079E-11	
19	15038999	17949773	3	gain	0.000428486	
19	23286192	35414417	3	gain	8.42123E-08	
19	35414417	35899546	4	gain	0.083665749	
20	0	31533385	3	gain	1.13541E-28	
20	31533385	63025520	4	gain	8.8168E-37	
21	0	16009257	3	gain	0.09964583	
22	0	22801063	1	loss	0.002311058	
22	37840062	41721094	1	loss	0.000121124	
22	45602126	51304566	1	loss	6.39001E-05	
X	0	155270560	3	gain	8.4876E-89	